

FIRST ANNUAL REPORT
NASA Research Grant NAG 8-684

Period of Performance
10-1-87 through 9-30-88

PROCESS MODELLING FOR
SPACE STATION EXPERIMENTS

Principal Investigators

FRANZ ROSENBERGER

J. IWAN D. ALEXANDER

(NASA-CR-183274) PROCESS MODELLING FOR
SPACE STATION EXPERIMENTS Annual Report No.
1, 1 Oct. 1987 - 30 Sep. 1988 (Alabama
Univ.) 51 p

CSCD 22A

G3/12

N89-10922

Unclass
0167513

Center for Microgravity and Materials Research
The University of Alabama in Huntsville
Huntsville, Alabama 35899

NAG8-684: Process modelling for Space Station experiments
Annual Report for the period 10-1-87 through 9-30-88

General Status

The work performed during the first year 10/1/87-9/30/88 involved analyses of crystal growth from the melt and from solution. The particular melt growth technique under investigation is directional solidification by the Bridgman-Stockbarger method. Two types of solution growth systems are also being studied. One involves growth from solution in a closed container, the other concerns growth of protein crystals by the hanging drop method. Following discussions with Dr. R. J. Naumann of the Low Gravity Science Division at MSFC it was decided to tackle the analysis of crystal growth from the melt earlier than originally proposed (see Task Schedule, section 2.3, page 12, of Proposal). Rapid progress has been made in this area. Work is on schedule and full calculations have been underway for some time. Progress has also been made in the formulation of the two solution growth models. More details are available in the following sections.

Numerical methods and code development

For all three model systems PHOENICS, a commercially available finite volume code, has been used extensively. In addition, a code has been developed, which employs a Chebyshev-collocation pseudo-spectral method, and applied to both steady and time-dependent cases for the analysis of crystal growth by the Bridgman-Stockbarger technique. This method has been used to verify our earlier calculations, increase accuracy (particularly in the vicinity of the solid-liquid interface) and to extend the range of parameter space under investigation. We are currently using this code, and are also processing the results of calculations carried out over the last few months. Preliminary results for thermosolutal convection have also been obtained and will be extended. Further calculations are also planned which will cover a wider range of parameter space and involve more realistic (g-jitter) disturbances.

Crystal growth from the melt by the Bridgman-Stockbarger method

The formulation of the model was completed during the first semi-annual period and progress in this area is advancing faster than originally anticipated. Preliminary results were reported in detail in the first semi-annual report and a publication is currently in preparation describing the first year's results.

The goal is to examine the effects of the microgravity environment on the compositional uniformity of crystals grown by the Bridgman-Stockbarger technique. In past space experiments this technique has been used for the directional solidification of crystals, and it is anticipated that this technique will be used in the Materials Technology Module (MTL) and the Materials Processing Facility (MMPF). During the first year our modelling efforts in this area have resulted in the development of two- and three- dimensional models of directional solidification which have been used to determine the sensitivity of crystal compositional uniformity to both time-dependent and steady residual accelerations. Selected results are described in detail in appendix A.

To date we have shown that:

a) A steady background level on the order of 10^{-6} - 10^{-5} g can be tolerated provided that the acceleration vector is *aligned with the axis of the growth ampoule*, and provided that no accelerations with frequencies less than 10^{-2} Hz (and amplitudes on the order of the steady component) are present.

b) For a fixed growth rate, the amount of lateral segregation is very sensitive to the orientation of the steady component of the residual gravity vector. The worst case appears to be when the acceleration vector is parallel to the crystal interface. At growth rates on the order of microns per second, this orientation leads to compositional non-uniformities of 22% when the magnitude of the acceleration is $\sqrt{2}(10)^{-6}$ g. If, however, the growth rate is lowered by an order of magnitude, the non-uniformity is reduced significantly (down to 4-5% in this case).

c) The response of the solute field, and the lateral non-uniformity, to oscillatory accelerations varies from no response at all (at frequencies above 1 Hz with amplitudes below 10^{-3} g), to a significant response at 10^{-3} Hz at amplitudes on the order of 10^{-6} g. In addition, additive effects were observed for combinations of a steady component and a low frequency component. These additive effects gave rise to significant lateral and *longitudinal* non-uniformities in concentration.

d) The effects of impulse-type disturbances can be severe and can extend for a long time (of order 10^3 seconds) after the termination of the impulse. For example a pulse with a one second duration, or a combination of such pulses has a drastic effect on the segregation levels at pulse amplitudes of 10^{-3} g. The nature of the response depends on the magnitude, direction and duration of the impulse, and whether sequential opposing impulses are involved. A so-called "compensating" double pulse will not result in completely offsetting effects. For the case we examined, however, the resulting compositional non-uniformity was not as severe as for sequential pulses with the same orientation. Further investigation of more realistic impulses is necessary since the response of the system appears to depend on the nature of the impulse and our results, and the results of others, indicate that impulses appear to have important consequences for transient behavior in crystal growth systems.

It should be borne in mind that to date our calculations have only covered a part of a large parameter space. In particular, it should be noted that for a given level of residual acceleration the amount of lateral segregation can be expected to increase with increasing Schmidt number (equivalent to increasing kinematic viscosity or decreasing solute diffusivity) and with decreasing distribution coefficient.

The consequences of variations in these parameters in relation to the type of time-dependent accelerations dealt with in this preliminary communication will be investigated as part of the ongoing research program.

Thermal convection in a square cavity

This work was carried out in order to investigate the reliability of order of magnitude estimates of the effects of residual accelerations on transport conditions in simple fluid systems.

The chosen systems involved thermal convection in square and rectangular cavities. The rigid upper and lower boundaries were maintained at constant but different temperatures. The temperature differences examined ranged from 5 K to 50 K over distances of 1-5 cm. The sidewalls were insulating. The applied residual gravity vector was time-dependent in both magnitude and orientation. Time dependent and steady accelerations were examined. It became readily apparent that while the fluid responded to the body force, the temperature field was relatively insensitive. At Prandtl numbers of order one the temperature field exhibited minor oscillations about the basic diffusion profile (a simple linear profile for this case). However, none of the cases examined showed a significant fluctuation in heat flux at the low temperature boundary. The major reason for this appears to be the strong influence of our thermal boundary conditions on the heat transfer rates in the system.

In order to check the reliability of order of magnitude estimates the g -sensitivity predicted by the Langbein-Tiby approach was also tested. The basic scenario is that described in their paper [1]. "In many fluid physics experiments, when particle motion is observed or the behavior of a growth front is studied, one can assume that $\delta r/r$ [the average density change] in the test volume has the order of magnitude 10^{-2}the diameter of the test volume is chosen to be 2 cm, temperature differences of 5 K are applied and an accuracy of $\delta T = 0.05$ K is required ..." In addition, we assumed adiabatic sidewalls.

The estimated tolerable g -level for the the above requirement is given as

$$a_{\max} = 2[\omega^2 + (\nu/L^2)^2]^{1/2} [\omega^2 + (\kappa/L^2)^2]^{1/2},$$

and is based on a "typical velocity" magnitude given by

$$O[|\mathbf{u}(\mathbf{r})|] = (\delta\rho/\rho) a_0 \omega^{-1} [\omega^2 + (\nu/L^2)^2]^{-1/2},$$

where ω is the frequency of the residual acceleration, the kinematic viscosity of the fluid is $\nu = 10^{-2} \text{ cm}^2 \text{ s}^{-1}$, $\kappa = 10^{-2} \text{ cm}^2 \text{ s}^{-1}$ is the

thermal diffusivity, L is the characteristic length (taken to be 2 cm) and a_0 is the magnitude of the acceleration. The predicted order of magnitude of the velocity u for a steady acceleration of $10^{-6} g$ is three orders of magnitude higher than the maximum velocity computed from the solution of the full non-linear equations. In every case we examined, the maximum velocity estimates were at least two to three orders of magnitude higher than our maximum computed velocities. As a consequence, the effect of residual accelerations tend to be overestimated. These discrepancies can be explained simply in terms of lack of a suitable length scale on which to base the estimates and the fact that order of magnitude estimates cannot, in general, properly account for the geometrical and thermal nature of the boundary conditions.

Effects on transport conditions during protein crystal growth via the hanging drop method

The starting point for this work is the simplified one-dimensional diffusive model of Fehribach and Rosenberger [2]. To examine the effects of residual acceleration on this type of crystal growth technique buoyancy driven convection must be included in the model. In addition, the nature of the interfacial conditions between the hanging drop, the "wall" to which it is partly attached and the vapor with which it is in contact, result in a complicated moving boundary problem which cannot be adequately handled using our available codes. Hence, development of a suitable numerical algorithm is in progress. The method under consideration involves a front fixing method [3], a finite difference approximation in space and an alternating direction implicit (ADI) method.

Transport conditions during crystal growth from solution

Triglycine sulphate crystals were grown from aqueous solutions on Spacelab 3 using the Fluid Experiment System (FES). Under the assumption of zero-gravity, Yoo et al. [4] have modelled the diffusive transport conditions for this system and estimate the influence of convection using order of magnitude considerations. Their results suggest that convective effects cannot be ignored.

In order to obtain more quantitative information concerning the effect of convection we have formulated a model based on that of Yoo et al. [4] but have included momentum as well as mass and heat transfer equations. As a practical measure the increase in computation consequent to the introduction of the momentum equation has been offset somewhat by simplifying the geometry of the computational domain.

Communications

Communications with MSFC personnel (Dr. R. J. Naumann and Mr. F. Rutledge) have taken place on a regular basis. A detailed semi-annual report was submitted in April 1988. Specific information was supplied to Dr. R. J. Naumann (MSFC) concerning microgravity requirements to be used in testimony to Congress.

Selected results of our analysis of the Bridgman-Stockbarger technique have been the subject of several presentations including the MSFC Distinguished Lecture Series, May 31st 1988 (given by Professor Rosenberger), and keynote presentation to the Microgravity Science and Space Experiments session at the 3rd International Conference on Drops and Bubbles in Monterey California September 19-22 1988.

Planned Work for the third six month period

During the first six months of the second year the analysis of crystal growth from the melt will be brought to completion. Work remaining to be done in this area includes a more detailed examination of thermosolutal convection and an examination of more realistic residual accelerations (g-jitter). During this period the preliminary stages of models for crystal growth from solution (closed container) will be completed and full scale calculations will begin.

References

- [1] R. Monti, J.J. Favler and D. Langbein, in Fluid Sciences and Materials Science in Space. A European Perspective, Ed. H. U. Walter (Springer, Berlin 1987) p. 637.

- [2] J. D. Fehribach and F. Rosenberger, *Analysis of Models for Two Solution Crystal Growth Problems*, to appear J. Crystal Growth 1988.
- [3] J. Crank, Free and Moving Boundary Problems (Clarendon Press, Oxford) 1984.
- [4] Hak-Do Yoo, W. R. Wilcox, Ravindra B. Lal and James D. Trollinger, *Modelling the Growth of Triglycine Sulfate Crystals in Space* preprint 1987.

APPENDIX A

Response of convective-diffusive transport to spatial and temporal variations in effective gravity

By J. IWAN D. ALEXANDER, JALIL OUAZZANI
AND FRANZ ROSENBERGER

Center for Microgravity and Materials Research
The University of Alabama in Huntsville, Huntsville Alabama 35899

The reduced gravity environment on board a spacecraft in low earth orbit gives materials scientists and fluid physicists the opportunity to undertake experiments under conditions that reduces or eliminates buoyancy driven fluid convection in comparison to earth based conditions. As a consequence, the relative importance of heat and mass transport by diffusion is increased. In crystal growth this might be expected to lead to a more uniform crystal composition than would be obtained under terrestrial conditions. The process of crystal growth by the Bridgman technique is chosen as a case study. Two and three dimensional numerical models are used to examine the response of heat, mass and momentum transport to conditions characteristic of the microgravity environment. It is shown that the orientation of the experiment with respect to the steady component of the residual gravity is a crucial factor in determining the suitability of the spacecraft as a means to suppress or eliminate unwanted effects caused by buoyant fluid motion. The process is also extremely sensitive to transient disturbances. For example, a 3×10^{-3} g impulse of one second duration acting parallel to the interface of a growing crystal produces a response in the solute field which lasts for nearly 2000 seconds. Consequently lateral and longitudinal compositional variations occur over a length of nearly 6 mm in the grown crystal.

1. Introduction

For over two decades, particularly since the operation of Skylab in the early seventies, the prospect of undertaking experiments aboard a spacecraft in low earth orbit has appealed to scientists from several disciplines for a variety of reasons. In addition to serving as useful base for cosmologists and astronomers, an orbiting spacecraft provides an opportunity to study physical phenomena in the absence of the 9.8 ms^{-2} (1 g) acceleration experienced in an earth based laboratory. The various phenomena that have been the subject of space experiments have been described in a number of recent books and articles (Abduyevsky 1985; Feuerbacher et al. 1986; Hazelrigg & Reynolds 1986; Walter 1987).

Physical systems which respond to buoyancy forces will exhibit different behavior in space than in an earth based laboratory. A simple example is the behavior of bubbles or liquid drops with densities that differ from the host liquid. At the earth's surface, these move up or down in response to gravitational acceleration. In a spacecraft they will no longer exhibit such predictable behavior. More complex examples include the surface shapes of liquid films, bridges and drops, and mass transfer in crystal growth systems (which we shall examine in this work). Under earth based conditions mass transfer conditions can be strongly affected by buoyancy driven convection in the (fluid) nutrient phase. In the reduced gravity environment of a space laboratory, mass transfer is more likely to be controlled by diffusion (Rosenberger 1979; Sekerka & Coriell 1979, Hurle et al. 1987).

As the number and level of sophistication of space experiments has increased, our understanding of the characteristics of the space laboratory environment has also changed. What was initially referred to as "zero-g" has become "micro-g" and more recently transient acceleration measurements revealed "milli-g" perturbations caused by crew activities, machinery vibrations, attitude changes etc. (Chassay & Schwaniger 1987) Indeed, it has become clear from measurements of the acceleration environment in the Spacelab (Chassay & Schwaniger 1987; Hamacher et al. 1987), that the residual gravity levels on board a spacecraft in low earth orbit can be significant and should be of

concern to experimenters who wish to take advantage of the low gravity conditions on future Spacelab missions and on board the planned Space Station. While accelerations may be orders of magnitude lower than that experienced at the earth's surface, they are nonetheless finite and, thus, pose potential problems for certain types of experiments.

To date, analyses of the effects of a low gravity environment have, with a few exceptions (Kamotani et al. 1981; Chang & Brown 1983; Polezhaev 1984; McFadden et al. 1988) been restricted to either idealized assumptions or order of magnitude estimates (Spradley et al. 1975; Camel & Favler 1984, 1986; Langbein 1984, 1987; Boudreault 1984; Monti & Napolitano 1984; Monti et al. 1987). The validity of the various estimates has only been demonstrated for a few special cases (Rouzaud et al. 1985).

As a case study, we examine the effects of time-dependent and spatial variations in the effective gravity vector on solute redistribution in a simplified model crystal growth by the Bridgman-Stockbarger technique. In section 2 we discuss the phenomenon of segregation which, when influenced by unsteady and spatially varying transport conditions in the nutrient, leads to undesirable compositional variations. In section 3 we discuss the basic heat, mass and momentum transport model of the Bridgman-Stockbarger technique. The results obtained from our numerical models of the effects of residual steady and time-dependent acceleration during the melt growth of a doped semi-conductor crystal are presented in section 4 and discussed in section 5. Our results show that for this specific directional solidification system, residual g-levels of $10^{-6} g$ are adequate only if an optimal alignment of the system with respect to the residual gravity vector is maintained.

1.2 Solute Redistribution

Consider a two component solution system. The equilibrium between the solid and liquid phases in such a system can be represented by a binary phase diagram (Chalmers 1977). Except for the case of either a pure or a congruently melting material, the

liquidus and solidus lines do not coincide. This is illustrated in Fig. 1 which depicts the equilibrium phase diagram for a solid solution of A-B where B is the dilute species (solute). The separation of liquidus and solidus indicates the compositional difference between the solid and the liquid with which it is in equilibrium. Such compositional changes on solidification occur in the majority of systems of interest to the materials science community, particularly those materials needed for device fabrication (Rosenberger 1979). During growth of crystals from melts containing two or more components this characteristic gives rise to a phenomenon termed *segregation* or *redistribution*.

Segregation is of great importance for many aspects of materials preparation (Wilcox 1971; Flemings 1974; Rosenberger 1979) including, for example, the purification of materials, or the predetermination of the composition of the nutrient phase in order to achieve the desired dopant distribution in the solid. When a solid phase is solidified from a melt with an initially uniform composition, the rate of advance of the solid into the liquid is rarely slow enough to allow the liquid phase to adjust its composition throughout in accordance with the equilibrium phase diagram. This is because the mass transfer rates in the liquid are typically slower than the solidification rate. As a consequence, while *local equilibrium* may persist at the phase boundary, compositional gradients will still be established in both the solid and liquid phases (see Fig. 2). For cases in which local equilibrium conditions prevail at the phase boundary the interfacial transfer of a component may be described in terms of the equilibrium distribution coefficient (Rosenberger 1979). For the dilute binary alloy illustrated in Fig. 1, this distribution coefficient is given by $k = c_s/c_M$, where c_s and c_M are respectively the solute (B) concentrations in the solid and liquid. The value of k reflects whether the solute is preferentially rejected or incorporated upon solidification. The equilibrium distribution coefficient depends only on the thermodynamic equilibrium properties of the system, and is independent of the mass transfer kinetics.

In order to predict the operating conditions under which desirable dopant uniformities can be obtained, for example for doped

semi-conductor crystals, it is necessary to understand the interplay between the various processes affecting mass transfer and their effect on the composition of the growing solid. For situations in which the equilibrium distribution coefficient reflects the local mass transfer conditions at the interface it is clear that any time dependence or non-uniformity in the growth rate and mass transfer conditions will result in compositional non-uniformities in the crystal.

It has been recognized for some time that convection in the nutrient phase can, in some cases, result in undesirable compositional variations in melt grown semi-conductor crystals (Pimpuktar & Ostrach 1981; Müller 1982; Müller et al. 1984). In many of these cases, for example growth by the Bridgman-Stockbarger technique, the convection is buoyancy driven (Langlois 1985). An attractive feature of the low effective gravity environment afforded by a spacecraft, is the possibility of substantially reducing or eliminating buoyancy driven convection, and thus creating diffusion controlled conditions (Hurle et al. 1987) which can favor compositional uniformity in the crystal. In the following model of crystal growth by the vertical Bridgman-Stockbarger technique we shall investigate the compositional inhomogeneities introduced into the crystal as a consequence of buoyancy driven convection under steady and time-dependent reduced gravity conditions.

2.1 The basic model

The basic setup to be considered is depicted in Fig. 3. It is based on a model used by Chang and Brown (1983). Directional solidification takes place as an ampoule is translated through fixed "hot " and "cold" zones. The zones are separated by a thermal barrier which is modelled using adiabatic sidewalls. The temperature conditions are chosen such that the upper and lower parts of the system are molten and solid, respectively. Translation of the ampoule is modelled by supplying a doped melt of dilute bulk composition c_∞ at a constant velocity V_M at the top of the computational space, and withdrawing a solid of composition c_s (which in general will be a function of both space and time) from the bottom. The crystal-melt interface is located

at a distance L from the top of the computational space. The temperature at the interface is taken to be T_M , the melting temperature of the crystal, while the upper boundary is held at a higher temperature T_H . In an actual experiment, owing to the finite length of the ampoule there is a gradual decrease in length of the melt zone during growth. In this model transient effects related to this change are ignored. Thus, it is assumed that the ampoule is sufficiently long for these effects to be negligible. The only transient effects to be considered will arise directly from the time-dependent nature of the residual gravity field. We also assume that the contribution of the solute (dopant) to convection is negligible. Convection is driven only by thermal gradients. It has been shown that curvature of the solid-liquid interface can result in significant lateral compositional non-uniformity (Coriell & Sekerka 1979; Coriell et al 1981). We wish to focus attention on the influence of convection on the composition of the crystal and thus, have chosen to examine the planar interface case. For the two-dimensional model the dilute binary melt is assumed to occupy a rectangular region Ω which is bounded by planar surfaces (see Figure 3). In the three-dimensional model the rectangular region is replaced by a circular cylinder with a diameter equal to L .

The governing equations are cast in dimensionless form using L , the effective melt length, κ/L (where κ is the melt's thermal diffusivity), $\rho_M \kappa^2 / L^2$, $T_H - T_M$, and c_∞ to scale the lengths, velocity, pressure, temperature and solute concentration, respectively. The dimensionless equations governing momentum, heat and solute transfer in the melt are

$$\frac{\partial \mathbf{u}}{\partial t} + (\text{grad } \mathbf{u}) \mathbf{u} = -\text{grad} p + \text{Pr} \Delta \mathbf{u} + \text{RaPr} \theta \mathbf{g}(t), \quad (1)$$

$$\text{div } \mathbf{u} = 0, \quad (2)$$

$$\frac{\partial \theta}{\partial t} + \mathbf{u} \cdot \text{grad } \theta = \Delta \theta, \quad (3)$$

$$\frac{\text{Sc}}{\text{Pr}} \left(\frac{\partial C}{\partial t} + \mathbf{u} \cdot \text{grad } C \right) = \Delta C, \quad (4)$$

where, $\mathbf{u}(\mathbf{x},t)$ represents the velocity, $\theta = (T(\mathbf{x},t) - T_M)/(T_H - T_M)$ the temperature (where $T_H - T_M$ is the temperature difference between the hot zone and the crystal interface) and C represents the solute concentration. The parameters $Pr = \nu/\kappa$, $Ra = g\beta(T_H - T_M)L^3/\kappa\nu$ and $Sc = \nu/D$ are respectively the Prandtl, Rayleigh and Schmidt numbers. The term $\mathbf{g}(t)$ in equation (1) represents the (time-dependent) gravity vector. The value of g in Ra is taken to be 980 cm s^{-2} , i.e. equal to the terrestrial acceleration. Thus, the magnitude of \mathbf{g} represents the ratio between the actual residual acceleration and g . Table 1 lists the forms of $\mathbf{g}(t)$ we have examined to date.

The following boundary conditions apply at the crystal-melt interface

$$\theta = 0, \quad (5)$$

$$\mathbf{u} \cdot \mathbf{N} = Pe/\sigma, \quad (6)$$

$$\mathbf{N} \times \mathbf{u} \times \mathbf{N} = \mathbf{0}, \quad (7)$$

$$\frac{\partial C}{\partial z} = \frac{PeSc}{Pr}(1-k)C, \quad (8)$$

where \mathbf{N} points into the crystal and is the unit vector perpendicular to the planar crystal melt interface, $Pe = V_M L/\kappa$ is the Peclet number, $\sigma = \rho_M/\rho_s$ and k is the distribution coefficient. We define the measure of compositional non-uniformity in the crystal at the interface to be the lateral range in concentration given by

$$\xi = \frac{(c_{s\max} - c_{s\min}) \times 100\%}{c_{av}},$$

where c_s is the (dimensional) solute concentration in the crystal, and c_{av} is the average concentration. At the "inlet" ($z=0$) the following boundary conditions are applied

$$\frac{\partial C}{\partial z} = \frac{PeSc}{Pr}(C-1), \quad (9)$$

$$\theta = 1, \quad (10)$$

$$\mathbf{u} \cdot \mathbf{N} = Pe\sigma, \quad (11)$$

$$\mathbf{N} \times \mathbf{u} \times \mathbf{N} = 0, \quad (12)$$

Equations (8) and (9) express conservation of mass at the crystal-melt interface and the "inlet" respectively. Equations (6) and (10) guarantee continuity of the melt with the crystal and with the supply of melt at the "inlet", while equations (7) and (11) ensure no-slip tangent to the interface and the top surface. At the side walls the following conditions are applied

$$\text{grad } C \cdot \mathbf{e}_w = 0, \quad \mathbf{u} \cdot \mathbf{N} = \text{Pe}\sigma, \quad \mathbf{e}_w \cdot \mathbf{u} = 0, \quad (13)$$

along with

$$\theta = 1, \quad (14)$$

in the isothermal zone and

$$\text{grad } \theta \cdot \mathbf{e}_w = 0, \quad (15)$$

in the adiabatic zone. Here \mathbf{e}_w is the normal to the ampoule wall.

While the above model does not strictly apply to a specific furnace (for example details of the heat transfer at the ampoule walls are neglected), it nonetheless serves as a reasonable "generic" model with which to carry out a preliminary analysis of a directional solidification experiment under conditions characteristic of the low gravity environment of space.

Our calculations are limited to thermo-physical properties corresponding to dilute gallium-doped germanium. The values of the thermo-physical properties and the associated dimensionless groups and operating conditions are given in Table 2. For all our calculations the length, L , of the furnace and the temperature difference $T_H - T_M$ were taken to be 1 cm and 115° C, respectively.

2.2 Method of solution

The governing equations were solved using the code PHOENICS (Spalding 1981; Rosten & Spalding 1986). PHOENICS embodies a finite volume or finite domain formulation (Patankar 1980). It represents the governing equations introduced in the previous section as a set of algebraic equations. These equations represent the consequence of integrating the differential equation over the finite

volume of a computational cell (and, for transient, problems over a finite time) and approximating the resulting volume, area and time averages by interpolation. For the 2-D calculations discussed in this report we employed a 40x39 grid. The 3-D calculations were performed in a circular cylindrical domain with 20 nodes in the radial direction, 12 in the azimuthal direction and 39 in the axial direction. We found that for the 2-D calculation less than 40 points in the direction parallel to the interface resulted in poor convergence of the solute field.

The scheme employed has the same accuracy as a finite difference scheme which is of the order Δx , where Δx is the distance between the grid nodes. The time scheme is implicit and thus unconditionally stable. However, small time steps are required to obtain accurate solutions. For highly non-linear flows the use of under-relaxation is necessary to eliminate divergence and to ensure good convergence of the solutions.

We compared our results (to be discussed in detail in the following sections) with the results of Chang and Brown's (1983) axisymmetric calculations. Our 3-D axisymmetric computations were found to be in agreement with their work. In addition we carried out full 3-D (*non-axisymmetric*) steady calculations in order to calibrate our 2-D results. For one set of examples we found that with $\sqrt{2}(10)^{-5}$ g parallel to the interface the percentage compositional non-uniformity predicted by the 2-D calculation ($\xi = 152\%$) was 50% higher than predicted by the full 3-D calculation. This difference may be attributed to the increased surface to volume ratio which increases the effect of the "no-slip" boundary condition. The presence of the rigid walls somewhat retards the flow and, thus, in comparison to the 2-D case, the degree of solute redistribution is decreased. A comparison between 2- and 3-D calculations for $\sqrt{2}(10)^{-6}$ g revealed no significant difference in ξ . At this magnitude of the gravity vector, convection is localized and weak. The increase in surface to volume ratio for this 3-D case has little influence on the transport conditions.

3. Results

3.1 Steady accelerations: 2-D

The temperature field (Figure 4.) was found to be insensitive to the slow convective flows. This is due to the low Prandtl number of the melt. Note that there are lateral as well as longitudinal temperature gradients in the system. The consequent density gradient is responsible for driving convection in the melt even when residual acceleration magnitudes are as low as 10^{-6} times that experienced under terrestrial conditions.

The amount of lateral concentration non-uniformity varied with both magnitude and orientation of the residual acceleration. When no residual acceleration is present the isoconcentrates are all parallel to the planar crystal-melt interface. Figures 5-8 illustrate the solute and velocity fields for two cases where the residual acceleration is parallel to the crystal-melt interface. The values of lateral non-uniformity ξ for these and other cases are listed in Table 3 along with the orientation and magnitude of the associated acceleration vector. For a given magnitude, accelerations oriented parallel to the crystal interface resulted in the maximum compositional non-uniformity.

For the purpose of comparison with results of calculations corresponding to terrestrial gravitational conditions we refer to the results of Chang and Brown (1983) for growth under axisymmetric conditions (i.e. gravity is parallel to the ampoule axis). Their results show that the amount of compositional non-uniformity in the crystal varies non-linearly with increasing magnitude of the gravity-vector. The maximum non-uniformity occurs at 10^{-2} g, an intermediate value between the value of gravitational acceleration experienced at the earth's surface, and the 10^{-6} - 10^{-5} g values characteristic of the quasi-steady component of the effective gravity in a spacecraft. Unless the acceleration is lowered (with respect to terrestrial conditions) by four orders of magnitude, the compositional uniformity may not be improved. Similarly, we have evaluated the conditions under which lateral non-uniformities are a maximum when the residual gravity vector is parallel to the interface. In this case, for the particular system under consideration, the maximum lateral non-uniformities will occur for accelerations of the order 10^{-4} g

3.2 Steady accelerations: 3-D

Five three-dimensional calculations were undertaken in order to examine the influence of a more realistic geometry. Three runs were axisymmetric, with \mathbf{g}_0 anti-parallel to the solidification direction. Two were fully three-dimensional with \mathbf{g}_0 parallel to the crystal-melt interface. The compositional non-uniformity ξ was found to be approximately 10% lower for the axisymmetric cases than for their 2-D analogs. These calculations were carried out for $\|\mathbf{g}\| = 10^{-4}$, 10^{-3} and 10^{-2} . The isoconcentrates in the crystal are shown in Figures 9 and 10 for a section cut perpendicular to the ampoule axis. The fully 3-D cases were carried out for $\|\mathbf{g}\| = \sqrt{2}(10)^{-5}$ and $\sqrt{2}(10)^{-6}$. At the higher value of the residual acceleration, $\xi = 91\%$, which is approximately half the 2-D value. At $\sqrt{2}(10)^{-6}$ g, $\xi = 26\%$. Thus, for this case, there was little difference between the 2 and 3-D predictions.

3.3 Time-dependent accelerations:

3.3.1 Single frequency; combined steady + single frequency accelerations

A number of different types of periodic disturbances were examined. Single frequency disturbances of the form $\mathbf{g}(t) = \mathbf{g}_0 + \mathbf{g}_n \cos(2\pi\omega_n t)$ were examined with $\mathbf{g}_0 = 0$, $\sqrt{2}(10)^{-6}$ and $\sqrt{2}(10)^{-5}$, oriented parallel to, perpendicular to and at 45° to the crystal-melt interface. The range of frequencies examined was $\omega_n = 10^{-4}$, 10^{-3} , 10^{-2} , 10^{-1} , 1 and 10 Hz. For frequencies greater than 10^{-2} Hz, there were no discernable effects on the solute fields. The velocity field did, however, respond to the oscillatory disturbances. For the case of 10^{-3} Hz (at 5×10^{-6} g) the response of the solute field was significant. Lateral and longitudinal non-uniformity levels in excess of 15% were calculated. Figures 11 and 12 show the lateral non-uniformity as a function of time, and highlight the additive effect of oscillatory and steady components of the residual acceleration.

The effect of a multiple frequency disturbance is illustrated in Figure 13. The acceleration has three components, consisting of steady and periodic contributions and has the form

$$\mathbf{g}(t) = \mathbf{g}_0 + \mathbf{g}_1 \cos(2\pi 10^{-3} t) + \mathbf{g}_2 \cos(2\pi 10^{-2} t),$$

where $\|\mathbf{g}_0\| = \sqrt{2}(10)^{-6}$, $\|\mathbf{g}_1\| = 3\sqrt{2}(10)^{-6}$ and $\|\mathbf{g}_2\| = 3\sqrt{2}(10)^{-5}$. The magnitude of ξ is seen to vary with the frequencies of the acceleration.

3.3.2 Impulse-type accelerations

Four cases of impulse-type disturbances were examined. All impulses were superimposed onto a steady background acceleration of $\sqrt{2}(10)^{-6} g$ which was oriented parallel to the crystal-melt interface. Of these the one second duration pulses had the most dramatic effects.

Figure 14 depicts the flow field immediately after a one second $3(10^{-3})g$ impulse oriented anti-parallel to the background acceleration. Figures 15-20 illustrate the development of the solute field following the impulse. Note that the effects are long lasting. The velocity field relaxes back to the initial state after some 300 seconds. The response of the solute field lags behind. The effect of the impulse is to initially re-orient the flow field (compare Figures 7 and 14). At first this has the effect of reducing the lateral compositional non-uniformity. After 45 seconds have elapsed since the termination of the impulse the composition nonuniformity is reduced to zero and subsequently increases in magnitude but has the opposite sense in comparison to the initial non-uniformity. This change in sense can be seen upon comparison of Figures 16 and 17. At approximately 260 seconds after the termination of the impulse the lateral segregation reaches a maximum value of 26%. It then decreases in value eventually reaching zero at 1017 seconds, changing sense and slowly increasing toward its initial steady level of 21.5% after more than 2000 seconds have elapsed.

A shorter duration (10^{-1} second) pulse resulted, 350 seconds after the termination of the pulse, in a maximum deviation of the lateral non-uniformity of only 5% from the initial steady level.

The effects of two one second pulses separated by one second were also calculated. The magnitude of the pulses was $3 \times 10^{-3} g$, and they were oriented parallel to the crystal interface. Their main effect

was to drive the lateral segregation from 21.5% (the initial value) to 76% after 225 seconds.

In addition double pulses were also examined. A pulse anti-parallel to the background steady acceleration followed by an equal but opposite pulse does not result in a "null" effect. While the flow generated by the first pulse is reversed by the second pulse there is a net flow following the termination of the second pulse. This flow is in the same sense as the initial steady flow and results in an increase of the lateral non-uniformity in composition to a maximum of 24% at 100 seconds, whereupon it decays slowly to its initial value.

4. Summary

The salient results of our calculations for materials with properties and growth conditions similar to those listed in Table 2 can be summarized as follows:

1) For a fixed growth rate, the amount of lateral non-uniformity in composition is very sensitive to the orientation of the steady component of the residual gravity vector. The worst case appears to be when the acceleration vector is parallel to the crystal interface. At growth rates on the order of microns per second, this orientation can lead to non-uniformities of 22% when the magnitude of the acceleration is $\sqrt{2}(10)^{-6}$ g. If, however the growth rate is lowered by an order of magnitude, the non-uniformity is reduced significantly (down to 4-5% in this case).

2) A steady background level on the order of 10^{-6} - 10^{-5} g can be tolerated provided that the acceleration vector is *aligned with the axis of the growth ampoule*, and provided that no accelerations with frequencies less than 10^{-2} Hz (and amplitudes of the order of the steady component) are present.

3) The response of the solute field, and the lateral non-uniformity, to oscillatory accelerations varies from no response at all (at frequencies above 1 Hz with amplitudes below 10^{-3} g) to a significant

response at 10^{-3} Hz at amplitudes on the order of 10^{-6} g. In addition, additive effects were observed for combinations of a steady component and low frequency components. These additive effects gave rise to significant lateral and *longitudinal* non-uniformities in concentration.

4) The effects of impulse-type disturbances can be severe and can extend for a long time (on the order of 10^3 seconds) after the termination of the impulse. For example a pulse with a one second duration, or a combination of such pulses has a drastic effect on the segregation levels at pulse amplitudes of 10^{-3} g. The nature of the response depends on the magnitude, direction and duration of the impulse, and whether sequential opposing impulses are involved. A so-called "compensating" double pulse will not result in completely offsetting effects. For the case we examined, however, the resulting compositional non-uniformity was not as severe as for sequential pulses with the same orientation. Further investigation of more realistic impulses (g-jitter) is necessary since the response of the system appears to depend on the nature of the impulse and our results indicate that impulses appear to have important consequences for transient behavior in crystal growth systems.

It should be borne in mind that our calculations have only covered a small part of a large parameter space. In particular, it should be noted that for a given level of residual acceleration the amount of lateral segregation can be expected to vary according to the magnitude of the Schmidt number and distribution coefficient k . We have also examined the effect of the growth rate and have found that a reduction in growth rate by an order of magnitude will result in a significant reduction in non-uniformity (for the range of parameters we have studied). This is consistent with the results of Adornato and Brown (1987).

Acknowledgements

This work was supported by the National Aeronautics and Space Administration (NAG8-684) and by the State of Alabama through the Center for Microgravity and Materials Research.

REFERENCES

- Adornato, P. M. and Brown, R. A. 1987 Convection and Segregation in directional solidification of dilute and non-dilute binary alloys: Effects of ampoule design. *J. Crystal Growth* **80**, 155-190.
- Abduyevsky, V.S. Grishin, S.D., Leskov, L.V., Polezhaev, V.E., & Savitchev, V.V., 1984 *Foundations of Space Manufacturing*, MIR Publishers Scientific, Moscow.
- Boudreault, R. Numerical simulation of convections in the μg environment. *Proc. 5th European Symposium Materials Sciences under Microgravity*, Schloss Elmau FRG November 1984, ESA SP-222, 259-264
- Camel, D. & Favier, J.J. 1986 Scaling analysis of convective solute transport and segregation in Bridgman crystal growth from the doped melt. *J. de Physique* **47**, 1001-1014.
- Chalmers, B. 1977 *Principles of Solidification*, Krieger Publishing Co.
- Chang, C.J. & Brown, R. A. 1983 Radial Segregation induced by natural convection and melt/solid interface shape in vertical Bridgman growth. *J. Crystal Growth* **63**, 353-364.
- Chassay, R. P. & Schwaniger, A. J. Jr. 1986 *Low g measurements by NASA*, NASA -TM 86585.
- Coriell, S. R., Boisvert, R. F., Rehm, R. G. & Sekerka R. F. 1981 Lateral solute segregation during directional solidification with a curved solid-liquid interface. *J. Crystal Growth* **54**, 167-175.
- Coriell S.R & Sekerka, R. F. 1979 Lateral solute segregation during unidirectional solidification of a binary alloy with a curved solid liquid interface. *J. Crystal Growth* **46**, 479-482.
- Feuerbacher, B. Naumann, R. J. & Hamacher H. 1986 *Materials sciences in space. A contribution to the scientific basis of space processing*, Springer-Verlag.
- Flemings M. 1974 *Solidification processing*, Mcgraw-Hill.
- Hamacher, H. Jilg, Mehrbold, R. U. 1987 Analysis of microgravity measurements performed during D-1. *Proc. 6th European symposium on materials sciences under microgravity conditions*, Bordeaux, France Dec 2-5 1986, ESA SP-256, 413-420.

- Hazelrigg, George A. & Reynolds, Joseph M. 1986 (editors) *Opportunities for Academic Research in a Low Gravity Environment* American Institute for Aeronautics and Astronautics Inc.
- Hurle, J. T., Müller, G. & Nitsche, R. 1987 Crystal growth from the Melt, in *Fluid Sciences and Materials Science in Space. A European Perspective.* (ed. Walter, H. U.) pp. 315-354, Springer-Verlag.
- Kamotani, Y., Prasad, A. & Ostrach, S. 1981 Thermal convection in an enclosure due to vibrations aboard a spacecraft. *AIAA Journal* **19**, 511-516.
- Langbein, D. 1984 Allowable g-levels for microgravity payloads, Final report for ESA contract No. 5.504/83/F/FS(SC) September 1984, pp.1-29 Batelle Frankfurt.
- Langbein, D. 1987 The sensitivity of liquid columns to residual accelerations. *Proc. 6th European symposium on materials sciences under microgravity conditions*, Bordeaux, France Dec 2-5 1986, ESA SP-256, 221-228.
- Langlois, W. E. 1985 Buoyancy driven flows in crystal growth melts. *Ann. Rev. Fluid Mech.* **17**, 191-215.
- McFadden, G. B. & Coriell, S. R. (to appear) Solutal convection during directional solidification in *Proc. 1st National Fluid Dynamics Congress*, Cincinnati, July 1988.
- Monti, R. 1987 *ESA Contract Report, R-66.525, Technosystems Report TS-7-87*, April 1987.
- Monti, R., Favier, J.J. & Langbein, D. 1987 Influence of residual accelerations on fluid physics and materials science experiments in *Fluid sciences and materials science in space, a European perspective.* (ed. H. U. Walter) pp. 637-680. Springer-Verlag.
- Monti, R. & Napolitano, L. g-level threshold determination, Final report for ESA, Contract no. 5.504/83/F/FS/SC Technosystems Report TS-7-84, June 1984.
- Müller G., 1982 Convection in melts and crystal growth, in *Convective transport and instability phenomena* (eds. Zierep J. and Oertel H.) pp. 441-468, Braun Verlag.
- Müller G., Neumann, G. & Weber, W. 1984 Natural convection in vertical Bridgman configurations. *J. Crystal Growth* **70**, 78-93.
- Patankar, S. V. 1980 *Numerical Heat Transfer and Fluid Flow* Hemisphere Publishing .

- Pimpuktar, S. M. & Ostrach S. 1981 Convective effects in Crystals grown from melt. *J. Crystal Growth* **55**, 614-.
- Polezhaev, V.I. 1984 Hydrodynamics, heat and mass transfer during crystal growth in *Crystals* **10** (ed. H. C. Freyhardt) pp. 87-150, Springer-Verlag
- Polezhaev, V. I., Lebedev A. P. & Nikitin, S. A., 1984 Mathematical simulation of disturbing forces and material science processes under low gravity, *Proc. 5th European symposium on materials sciences under microgravity*, Schloss Elmau FRG, ESA SP-222, 237.
- Rouzaud, A., Camel, D. & Favier, J.J. 1985 A comparative study of convective solute transport and segregation in Bridgman crystal growth from the doped melt. *J. Crystal Growth* **73**, 149-166.
- Rosenberger, F. 1979 *Fundamentals of Crystal Growth I*. Springer Series in Solid-State Sciences, Vol. 5, Springer-Verlag.
- Rosten, H. I. & Spalding, D. B. 1986 Numerical simulation of fluid flow and heat and mass transfer processes, in *Lecture Notes in Engineering* (eds. C. A. Brennia and S. A. Orszag) Vol 18, pp. 3-29, Springer Verlag.
- Sekerka, R. F. & Coriell S. R., 1979 Influence of the space environment on some materials processing phenomena *Proc. 3rd European symposium on materials sciences in space*, Grenoble France, April 1979, ESA SP-142, 55-65.
- Spalding, D. B. 1981 A general purpose computer program for multi-dimensional one- and two-phase flow. *Mathematics and computers in simulation* Vol. XXIII North Holland Press 267-268.
- Spradley, L. W. Bourgeois, S. W. & Lin, F. N. 1975 Space processing convection evaluation, g-jitter of confined fluids in low gravity, *AIAA Paper No.* 75-695.
- Walter, H. U. 1987, editor. *Fluid Sciences and Materials Science in Space. A European Perspective*. Springer-Verlag.
- Wilcox, W. A. 1971 The role of Mass transfer in crystallization processes, in *Preparation and Properties of Solid State Materials*, (ed. R. A. Lefever) Marcel Dekker.

TABLE 1

Selected forms of the acceleration vector examined in this work.

Steady

$$\mathbf{g}_0 = g_{0x} \mathbf{i} + g_{0z} \mathbf{k};$$

$$\|\mathbf{g}\| = \sqrt{2}(10)^{-5}, 5\sqrt{2}(10)^{-6}, \sqrt{2}(10)^{-6}, \sqrt{2}(10)^{-7}$$

Time dependent

$$\mathbf{g}(t) = \mathbf{g}_0 + \mathbf{g}_n \cos(2\pi\omega_n t); \mathbf{g}(t) = \mathbf{g}_0 + \sum \mathbf{g}_n \cos(2\pi\omega_n t);$$

$$\omega_n = 10^{-4}, 10^{-3}, 10^{-2}, 10^{-1}, 1, 10 \text{ Hz},$$

$$\|\mathbf{g}_n\| = \sqrt{2}(10)^{-5}, 5\sqrt{2}(10)^{-6}, \sqrt{2}(10)^{-6}$$

Impulse

$$\mathbf{g}(t) = \mathbf{g}_b \quad t < t_1, \quad \mathbf{g}(t) = \mathbf{g}_b + \mathbf{g}_1, \quad t_1 < t < t_2, \quad \mathbf{g}(t) = \mathbf{g}_b \quad t > t_2$$

















$$\mathbf{g}_b = \sqrt{2}(10)^{-6}, \quad \mathbf{g}_1 = 3\sqrt{2}(10)^{-3}$$

TABLE 2

Thermo-physical properties characteristic of gallium-doped germanium (after Chang & Brown 1983) and operating conditions

Property	Value
Thermal conductivity of the melt	$0.17 \text{ WK}^{-1} \text{ cm}^{-1}$
Heat capacity of the melt	$0.39 \text{ Jg}^{-1} \text{ K}^{-1}$
Density of the melt	5.6 g cm^{-3}
Density of the solid	5.6 g cm^{-3}
Kinematic viscosity of the melt (ν)	$1.3 (10)^{-3} \text{ cm}^2 \text{ s}^{-1}$
Melting temperature (T_M)	1231 K
Solute diffusivity (D)	$1.3(10)^{-4} \text{ cm}^2 \text{ s}^{-1}$
Thermal diffusivity of the melt (κ)	$1.3(10)^{-1} \text{ cm}^2 \text{ s}^{-1}$
Segregation coefficient (k)	0.1
Thermal expansion coefficient (β)	$2.5 (10)^{-4} \text{ K}^{-1}$
Operating conditions	
Hot zone temperature (T_H)	1346 K
Distance between inlet and interface (L)	1 cm
Height of adiabatic zone	2.5 mm
Ampoule width (diameter)	1 cm
Translation (supply) rates (V_M)	$6.5 \mu\text{m s}^{-1}, 0.65 \mu\text{m s}^{-1}$
Associated dimensionless parameters	
Prandtl number $Pr = \nu/\kappa$	0.01
Peclet number $Pe = V_M L/\kappa$	$5(10)^{-3}$ and $5(10)^{-4}$
Schmidt number $Sc = \nu/D$	10
Density ratio σ	1.0

TABLE 3
Compositional non-uniformity ξ [%] for computed 2-D (3D)
steady state cases

Residual Acceleration Magnitude	Orientation		Ampoule Width 1 cm			2 cm	0.5 cm
	N	e_g	Growth Rate [$\mu\text{m s}^{-1}$]			6.5	6.5
			6.5	3.25	0.65		
$10^{-4} g$			36				
$10^{-4} g$			32				
$\sqrt{2}(10^{-5}) g$			110				
$\sqrt{2}(10^{-5}) g$			152				
			(91)				
							12
$10^{-5} g$							
$10^{-5} g$			7.5	4.6	0.7		
$5\sqrt{2}(10^{-6}) g$			57				
$\sqrt{2}(10^{-6}) g$			10				
$\sqrt{2}(10^{-6}) g$			22				
			(26)				
$\sqrt{2}(10^{-6}) g$			4.0				
$\sqrt{2}(10^{-6}) g$			2.0				
$10^{-6} g$			0.7	0.4	0.0	3.8	
$10^{-7} g$			1.0	0.5	0.2		

$e_g \equiv$ unit vector parallel to g , $N \equiv$ normal vector to interface pointing into melt, $H = 1$ cm for all cases

FIGURE CAPTIONS

- Figure 1. The temperature -composition phase diagram for a dilute binary system A-B, where B is the dilute species. The compositions in the solid (S) and liquid (L) are respectively given by c_s and c_m . The equilibrium distribution coefficient, k , is given by the XY/XZ .
- Figure 2. Concentration profiles in the liquid and solid caused by segregation:
- a) The zero growth rate (equilibrium) case.
 - b) In this case the solute is rejected at finite growth velocities. This results in compositional gradients in both phases.
- Figure 3. The prototype directional solidification model.
- Figure 4. The dimensionless temperature field, θ , for all 2-D cases discussed in this paper.
- Figure 5. The steady flow field produced by a residual acceleration with a magnitude $\sqrt{2}(10)^{-5} g$ acting parallel to the crystal melt interface. The maximum speeds are approximately twice the growth speed.
- Figure 6. The dimensionless solute field, C , associated with the flow depicted in Figure 5. For this case $\xi = 152\%$.
- Figure 7. The steady flow field produced by a residual acceleration with a magnitude $\sqrt{2}(10)^{-6} g$ acting parallel to the crystal melt interface. The maximum speeds are slightly greater than the growth speed.
- Figure 8. The dimensionless solute field, C , associated with the flow depicted in Figure 7. For this case $\xi = 22\%$.
- Figure 9. The steady solute distribution ($C_s = c_s/c_\infty$) in the crystal consequent to $\sqrt{2}(10)^{-5} g$ acceleration oriented parallel to the interface for the 3-D case. The cross section is taken perpendicular to the ampoule axis. $\xi = 91\%$.

- Figure 10. The steady solute distribution ($C_s = c_s/c_\infty$) in the crystal consequent to $\sqrt{2} (10)^{-6} g$ acceleration oriented parallel to the interface for the 3-D case. The cross section is taken perpendicular to the ampoule axis. $\xi = 26\%$.
- Figure 11. Lateral non-uniformity in composition, ξ , plotted as a function of time for an oscillatory residual acceleration with a maximum magnitude of $3\sqrt{2}(10)^{-6} g$ and a frequency of 10^{-3} Hz , acting parallel to the crystal-melt interface. The initial state was purely diffusive.
- Figure 12. Lateral non-uniformity in composition, ξ , plotted as a function of time for a residual acceleration consisting of a steady part with a magnitude of $\sqrt{2}(10)^{-6} g$ and an oscillatory part with a maximum magnitude of $3\sqrt{2}(10)^{-6} g$ and a frequency of 10^{-3} Hz , acting parallel to the crystal-melt interface. The calculation was started from a steady flow associated with a $\sqrt{2}(10)^{-6} g$ acceleration acting parallel to the interface.
- Figure 13. Lateral non-uniformity in composition, ξ , plotted as a function of time for a multi-component disturbance consisting of a steady low g background plus two periodic components: $\mathbf{g}(t) = \mathbf{g}_0 + \mathbf{g}_1 \cos(2\pi 10^{-3}t) + \mathbf{g}_2 \cos(2\pi 10^{-2}t)$, where $\|\mathbf{g}_0\| = \sqrt{2}(10)^{-6}$, $\|\mathbf{g}_1\| = 3\sqrt{2}(10)^{-6}$ and $\|\mathbf{g}_2\| = 3\sqrt{2}(10)^{-5}$. The calculation was started from a steady flow associated with a $\sqrt{2}(10)^{-6} g$ acceleration acting perpendicular to the interface.
- Figure 14. The velocity field after a one second pulse of $3(10)^{-3} g$ superimposed on a steady flow caused by a $\sqrt{2}(10)^{-6} g$ acceleration, both parallel to the crystal melt interface. The impulse, \mathbf{g}_I , is in the opposite direction to the background acceleration, \mathbf{g}_B . Note that the maximum velocity magnitudes are of the order $3(10)^{-2} \text{ cm s}^{-1}$ i.e. about 500 times those in Figure 7.

- Figure 15. Dimensionless solute field, C , immediately after the termination of the impulse. The compositional non-uniformity, ξ , is 21.5%.
- Figure 16. Dimensionless solute field, C , 31 seconds after the termination of the impulse. The compositional non-uniformity, ξ , is 6.1%.
- Figure 17. Dimensionless solute field, C , 81 seconds after the termination of the impulse. The compositional non-uniformity, ξ , is 11.4% and has changed sense.
- Figure 18. Dimensionless solute field, C , 431 seconds after the termination of the impulse. The compositional non-uniformity, ξ , is 21.7%.
- Figure 19. Dimensionless solute field, C , 881 seconds after the termination of the impulse. The compositional non-uniformity, ξ , is 4.5%.
- Figure 20. Dimensionless solute field, C , 1781 seconds after the termination of the impulse. The compositional non-uniformity, ξ , is 12.5%.

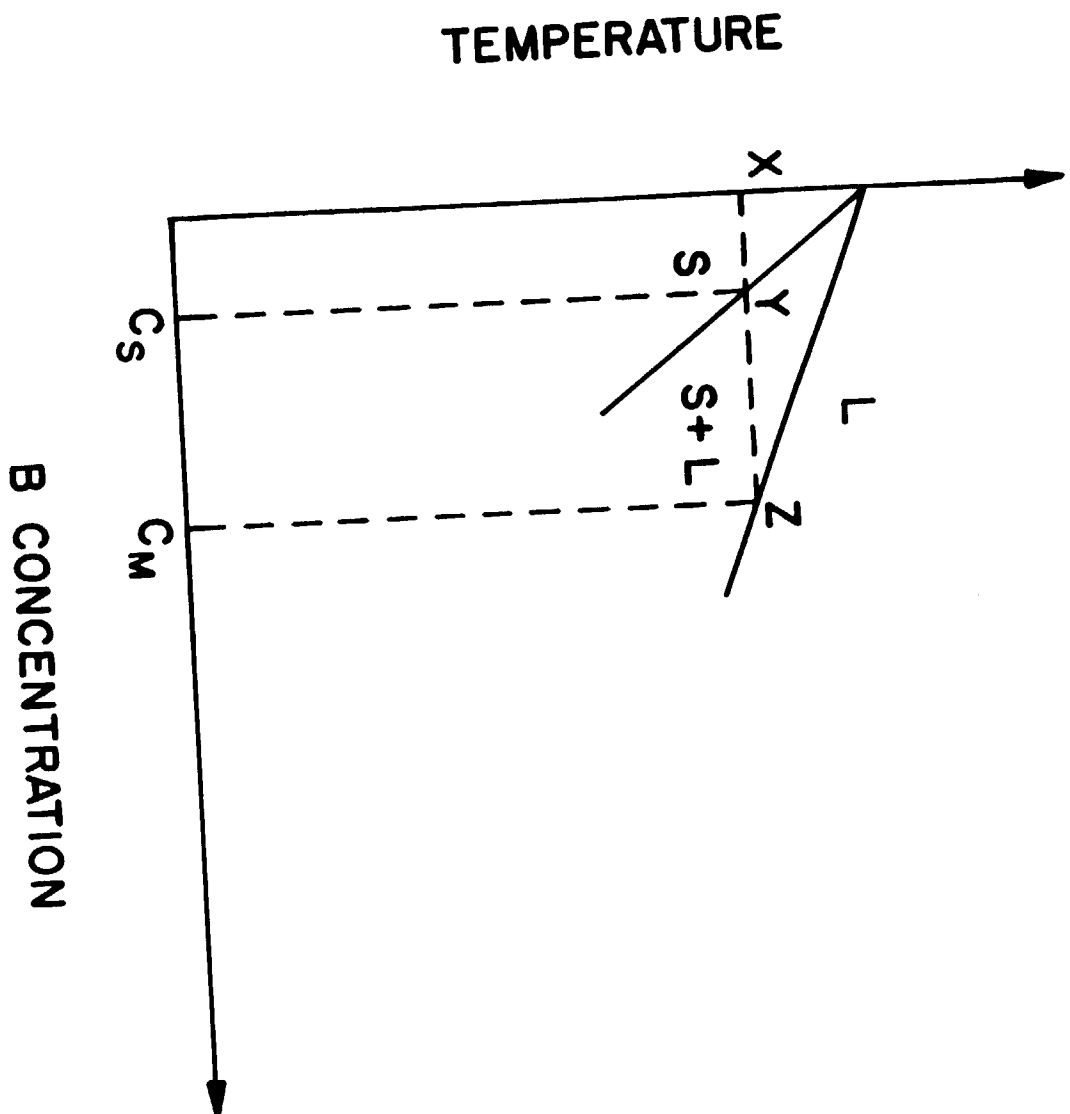


Fig 1

SEGREGATION

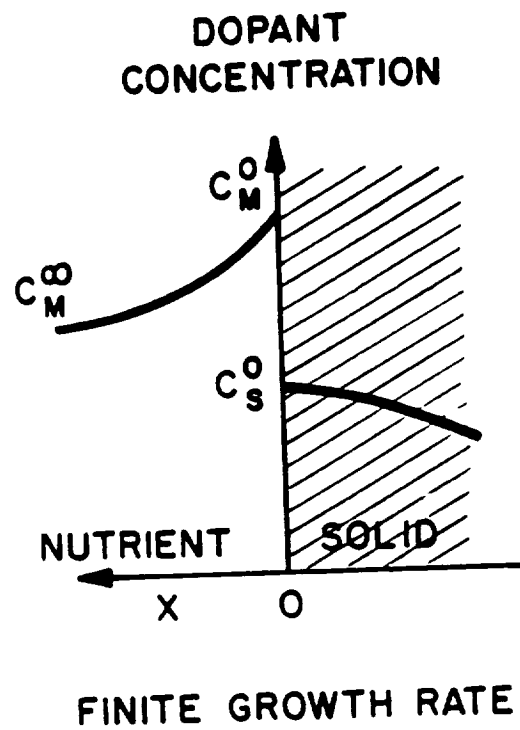
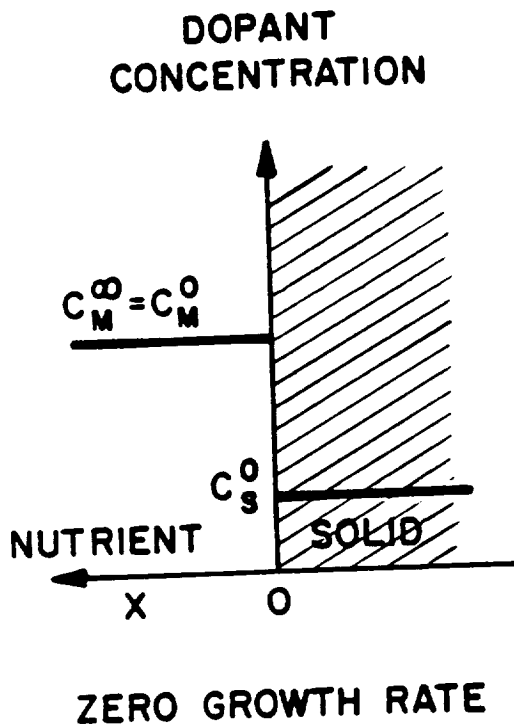


FIG.2.

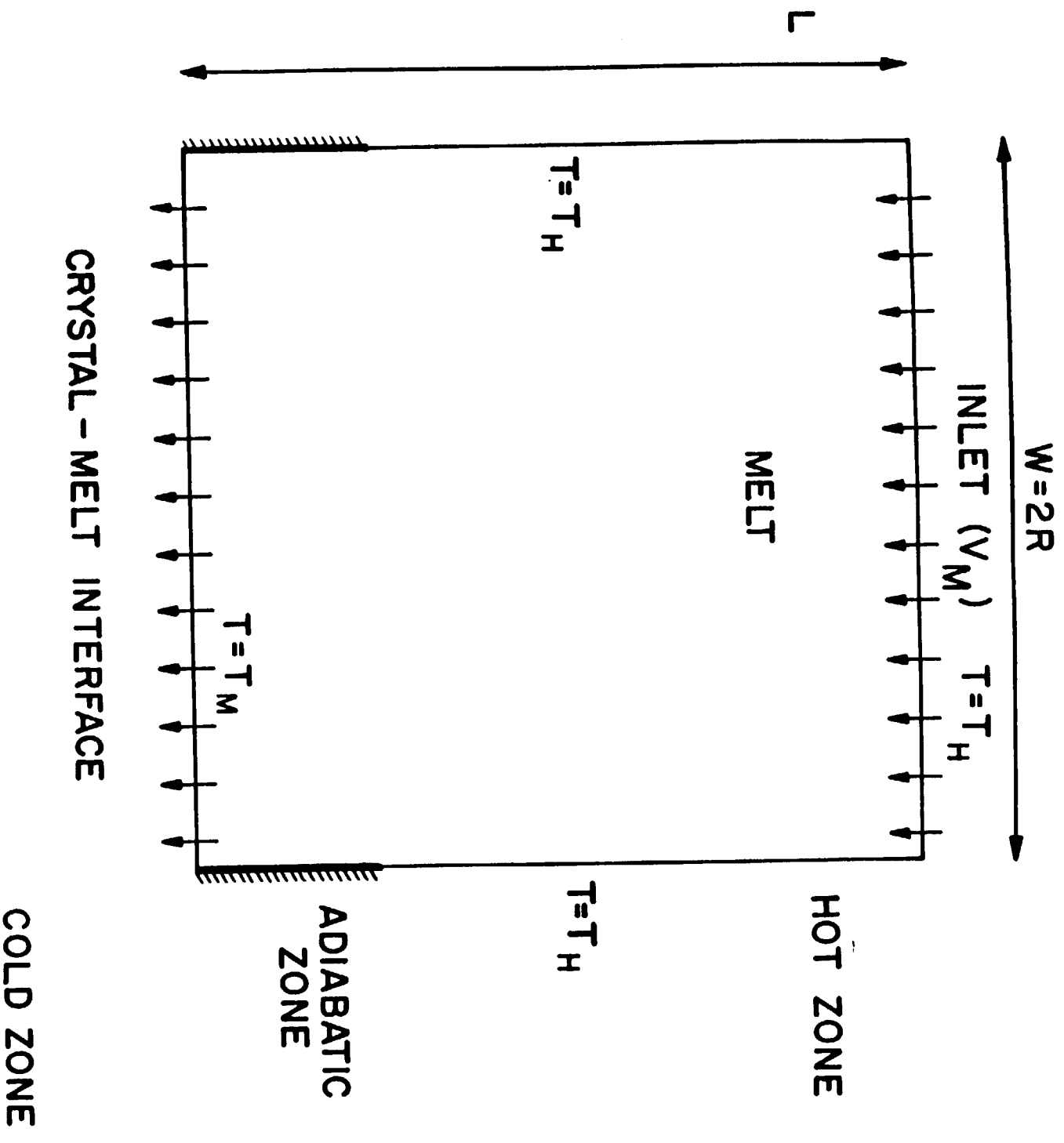


Fig. 3

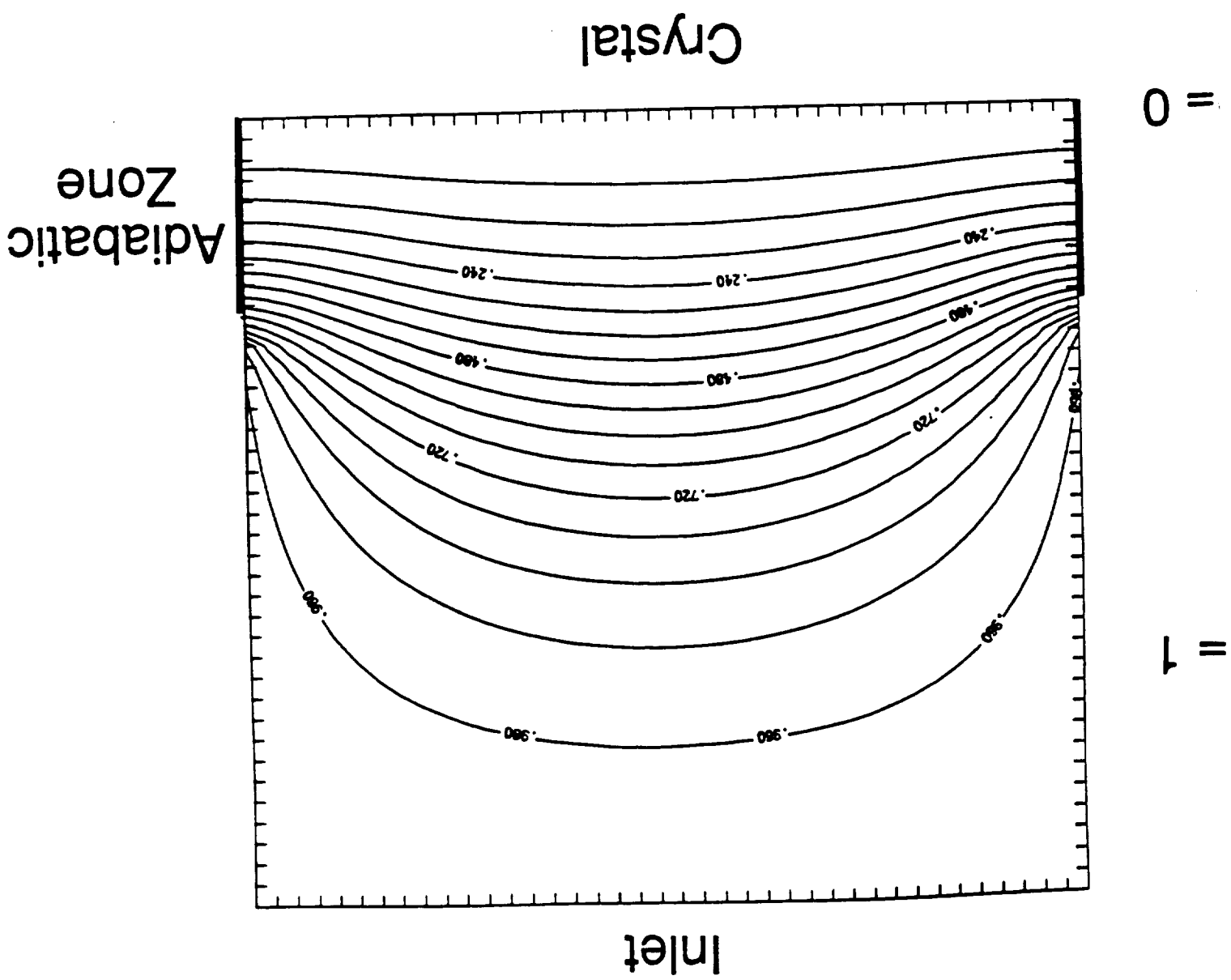


Fig. 4

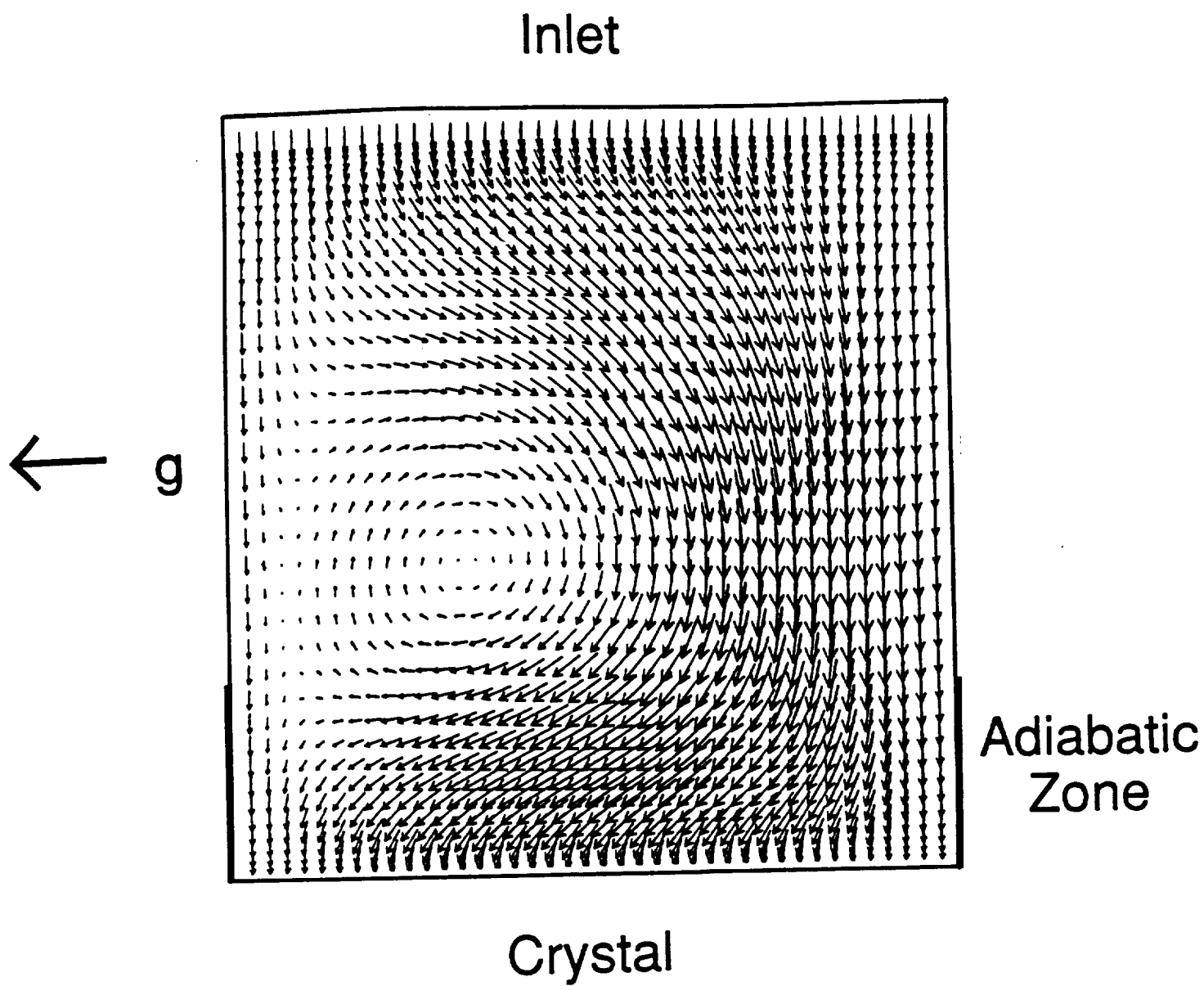


FIG. 5.

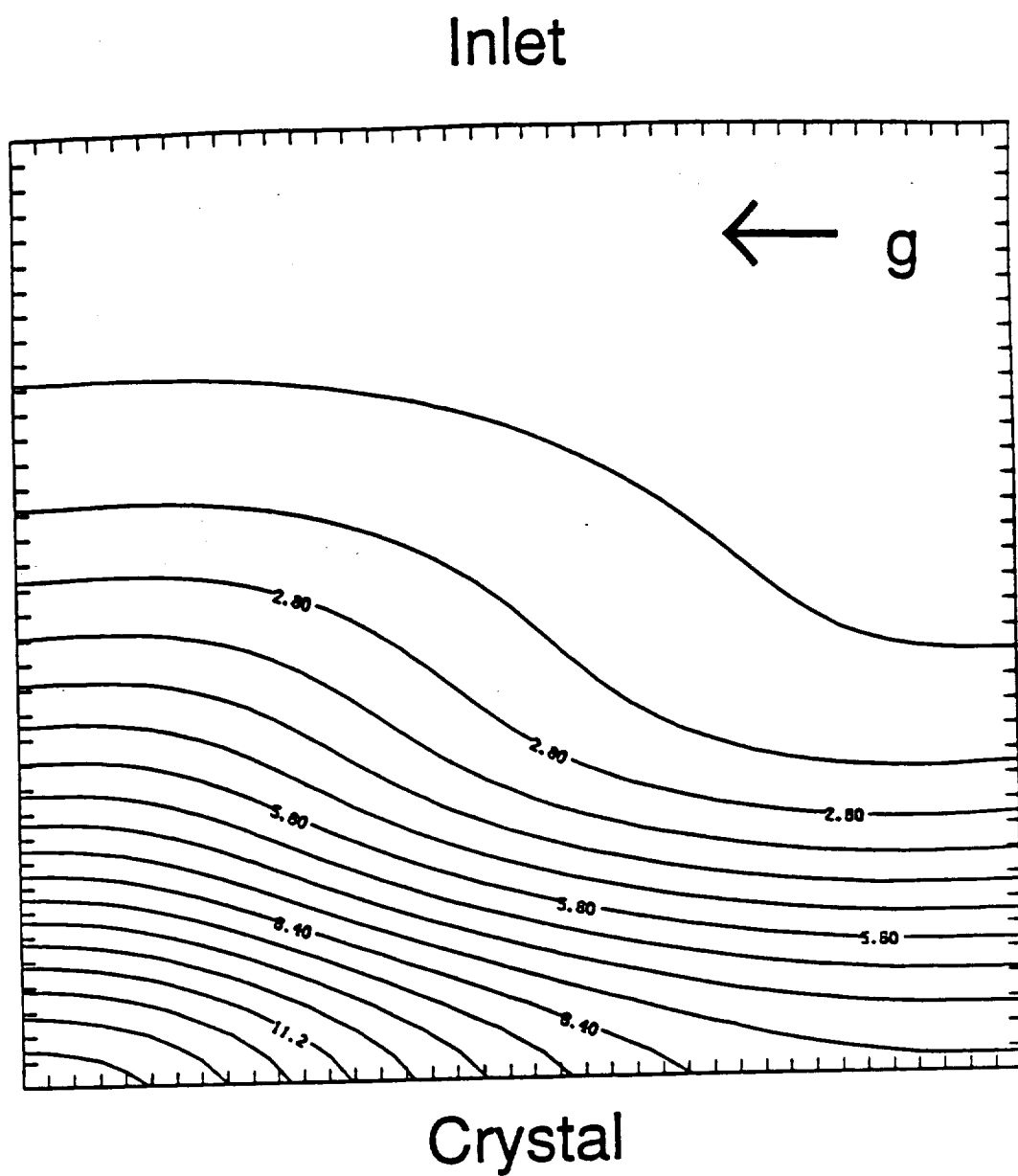


FIG. 6

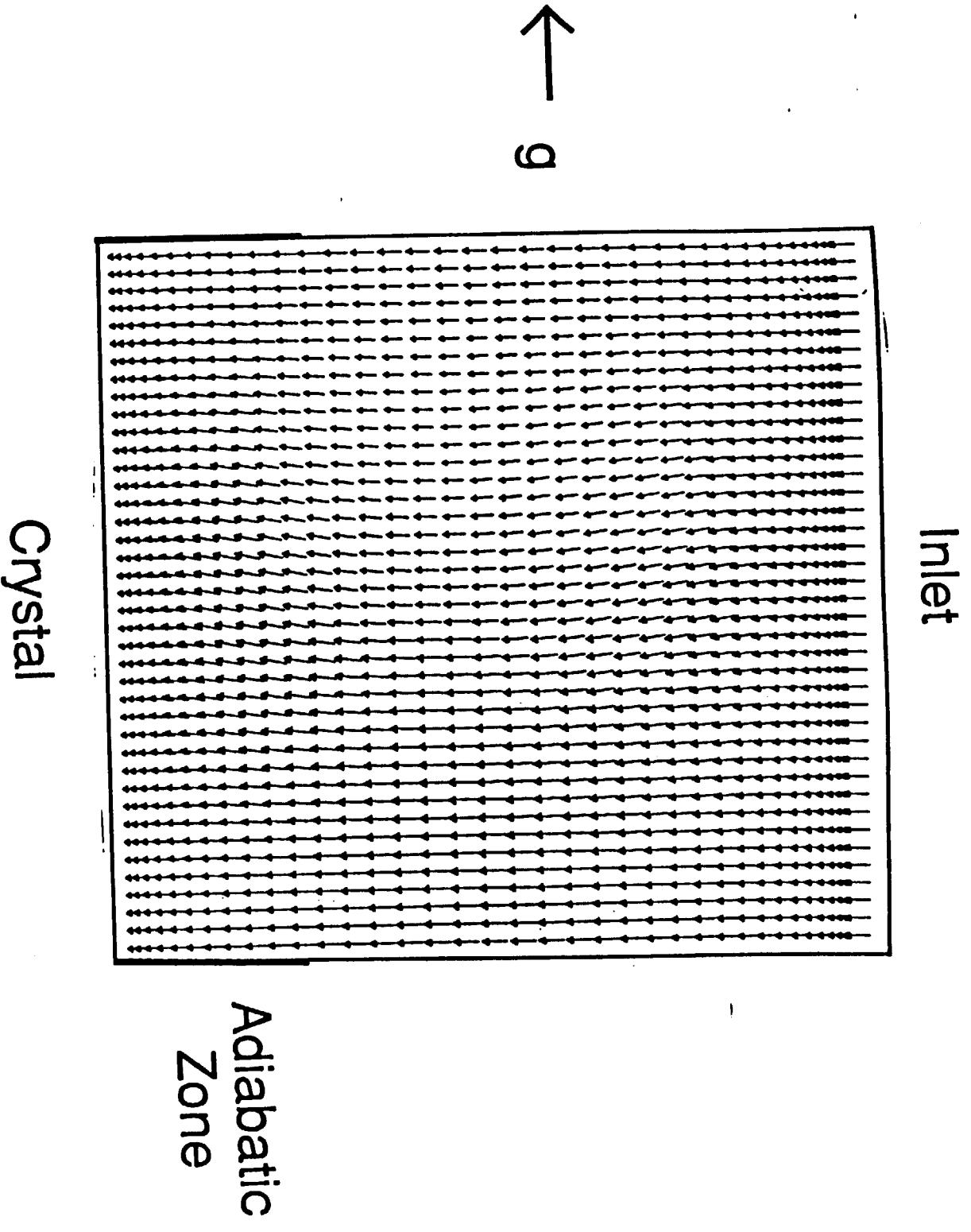


FIG. 7

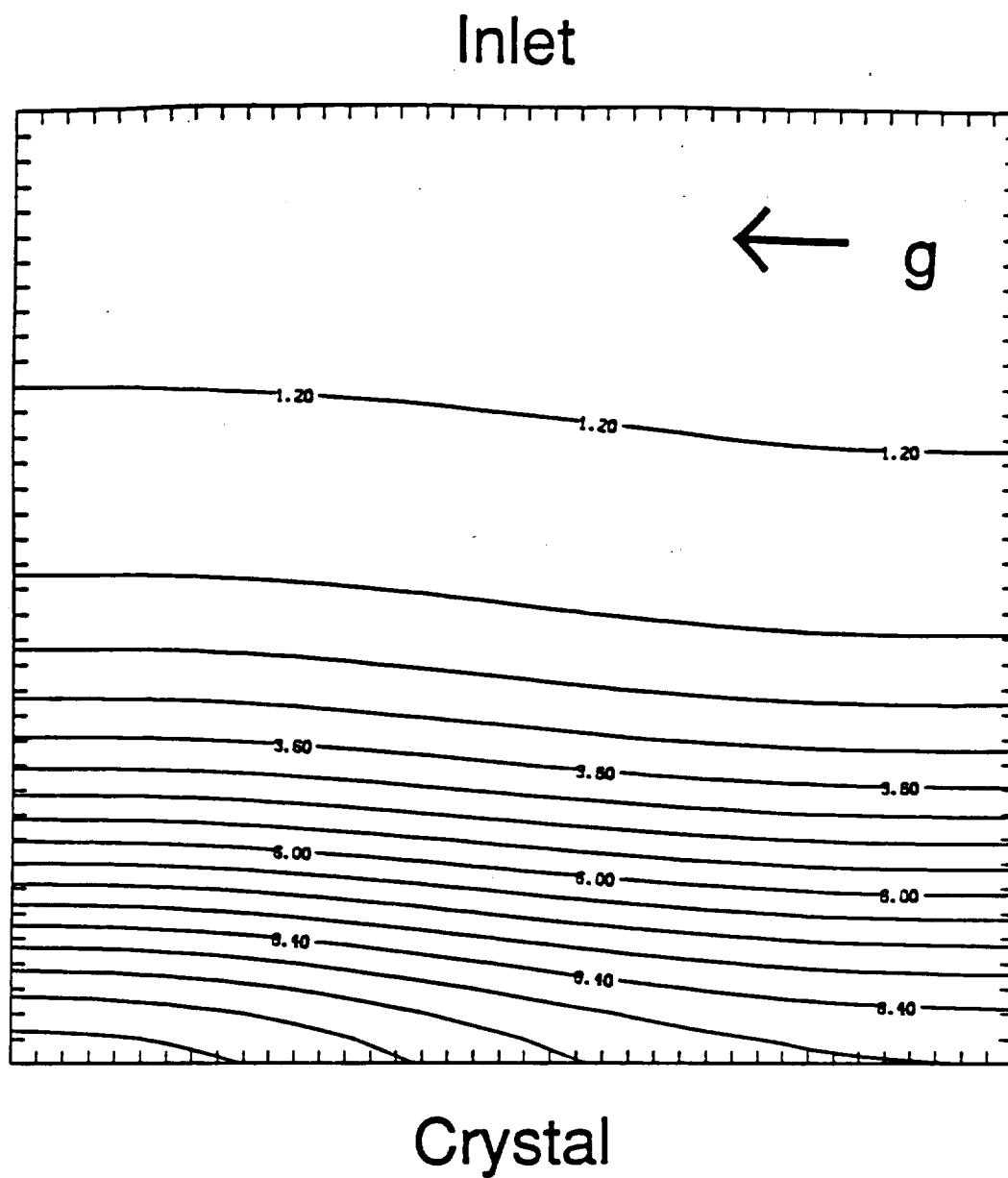


FIG. 8

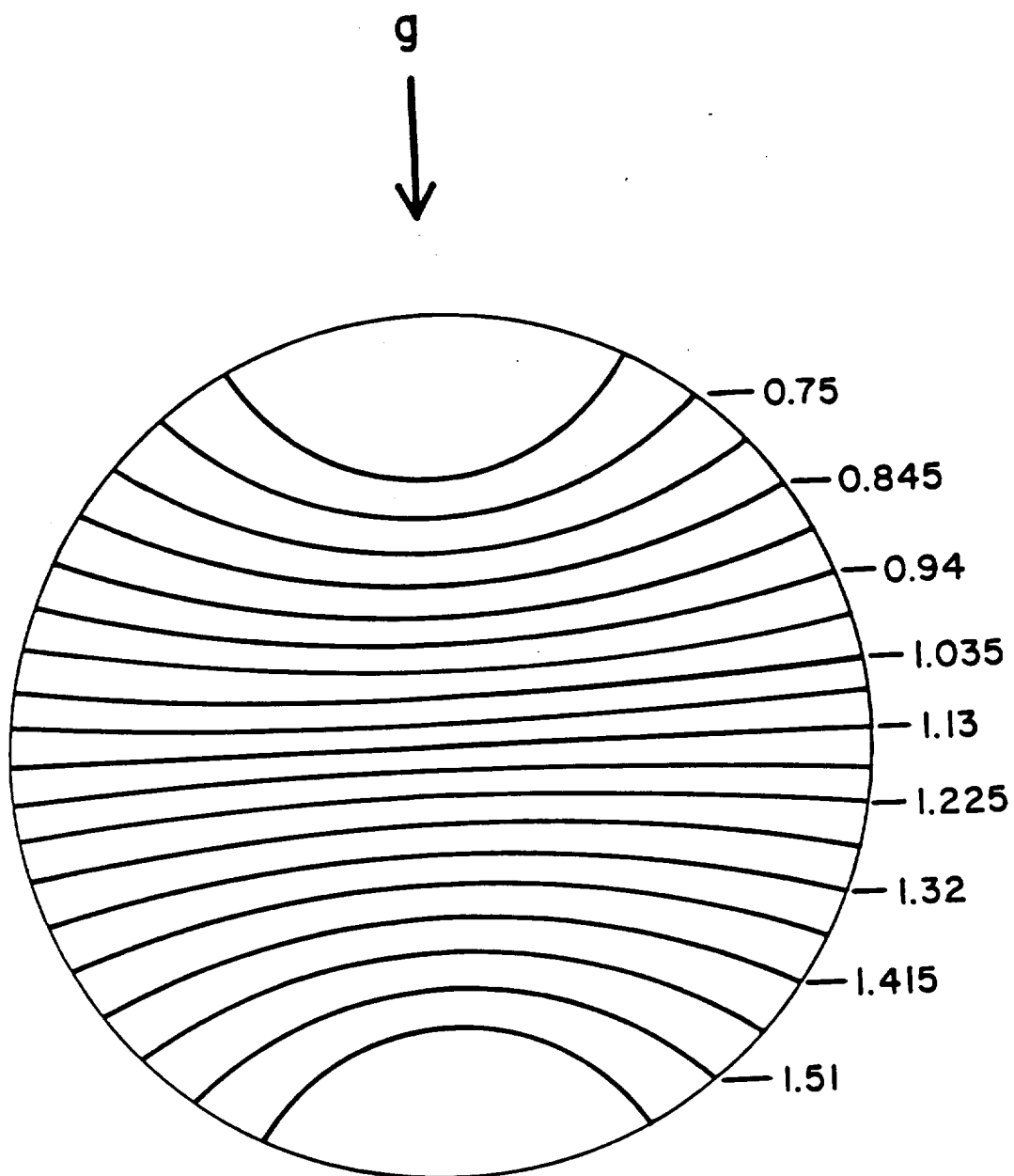


FIG. 9

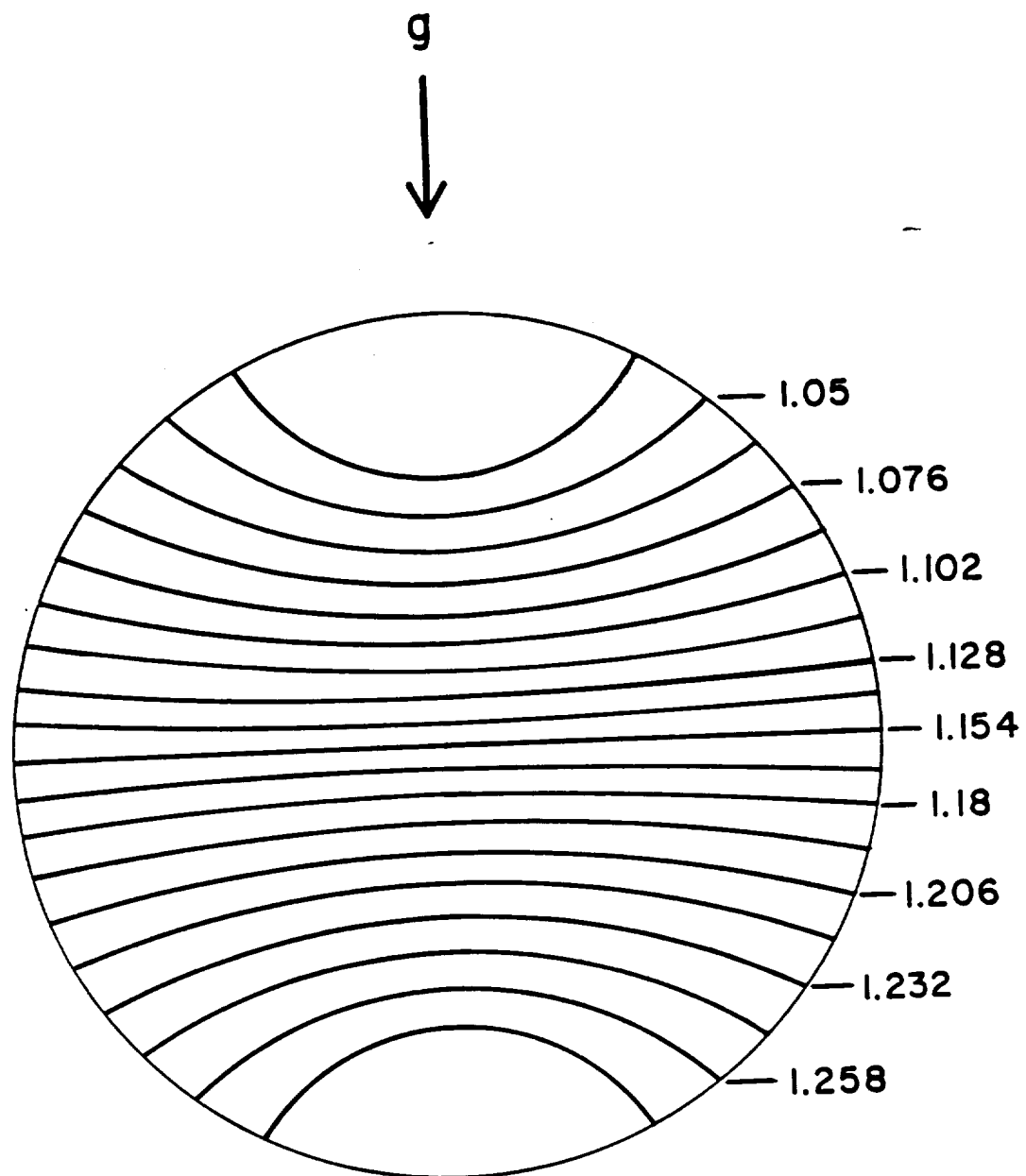


FIG. 10

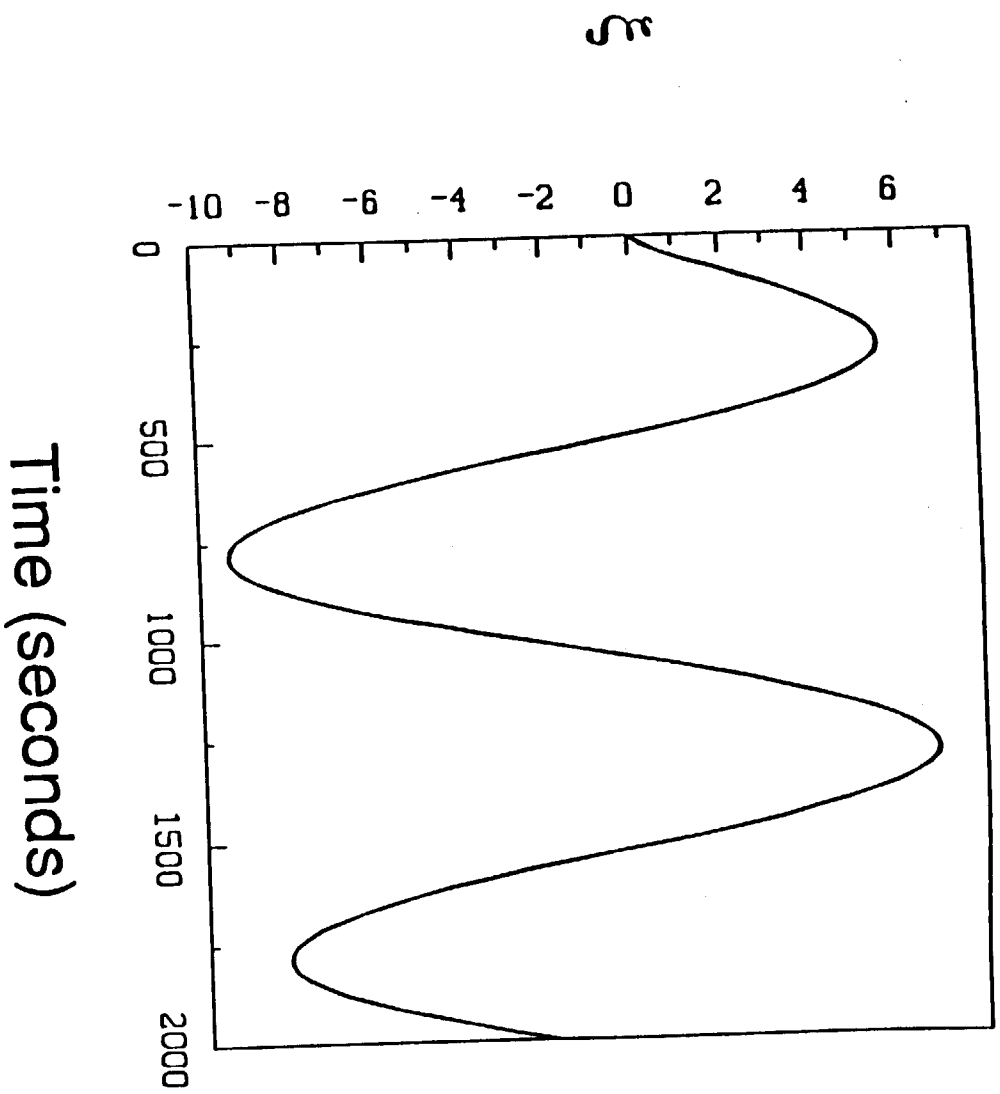


FIG. 11

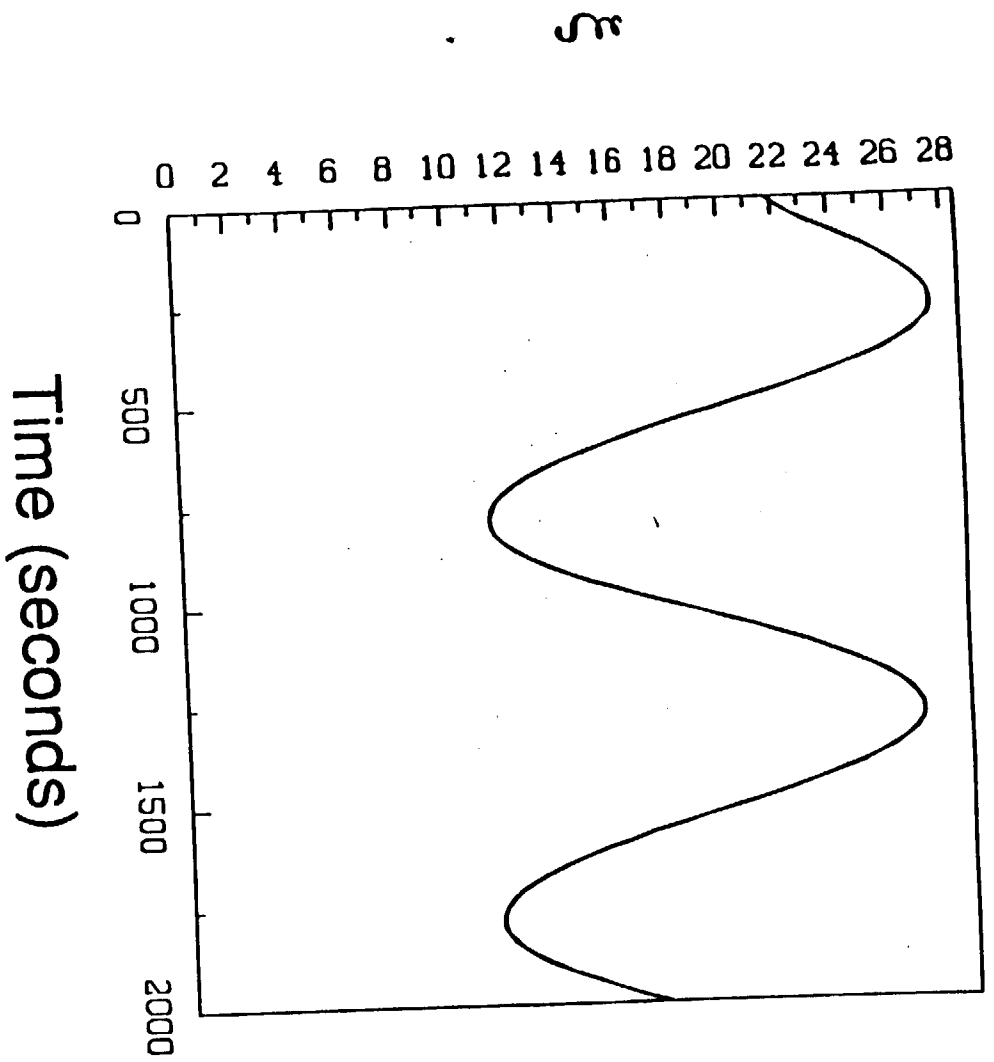


FIG. 12

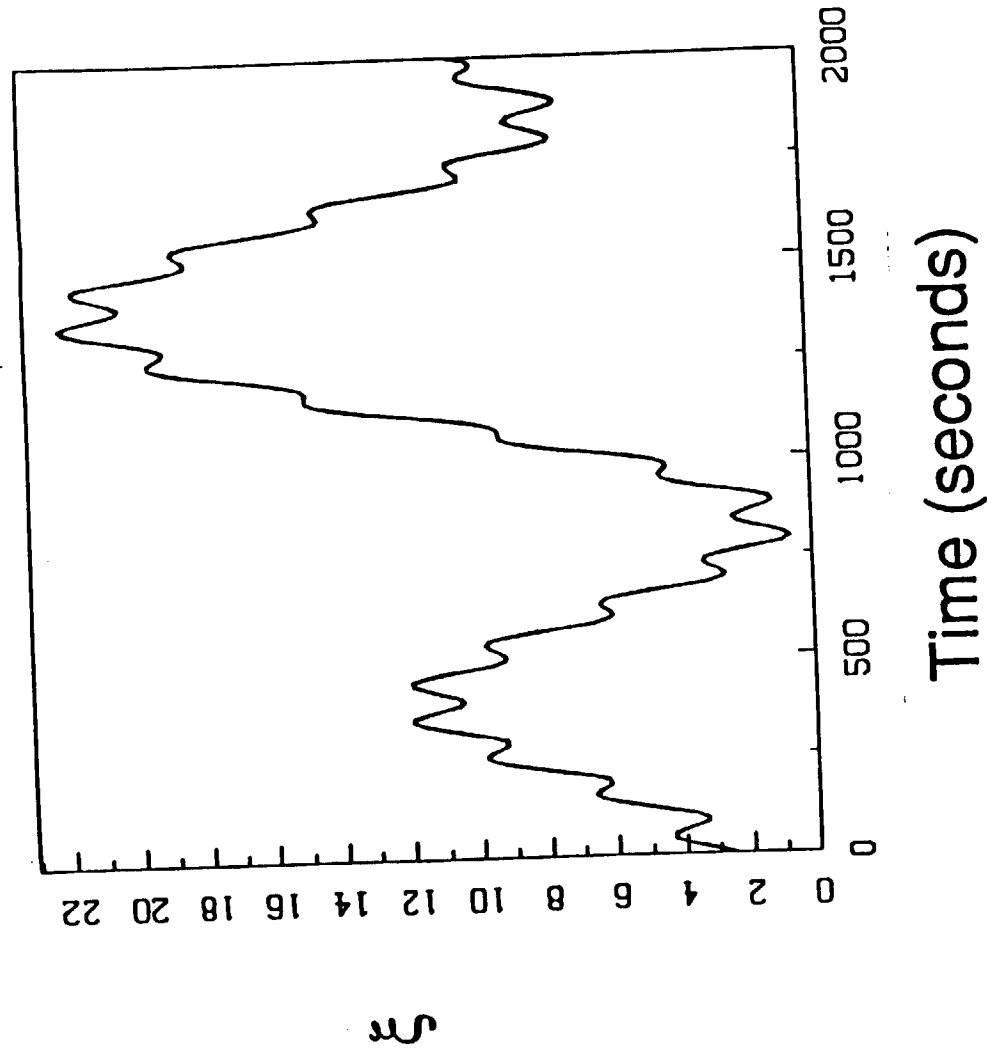
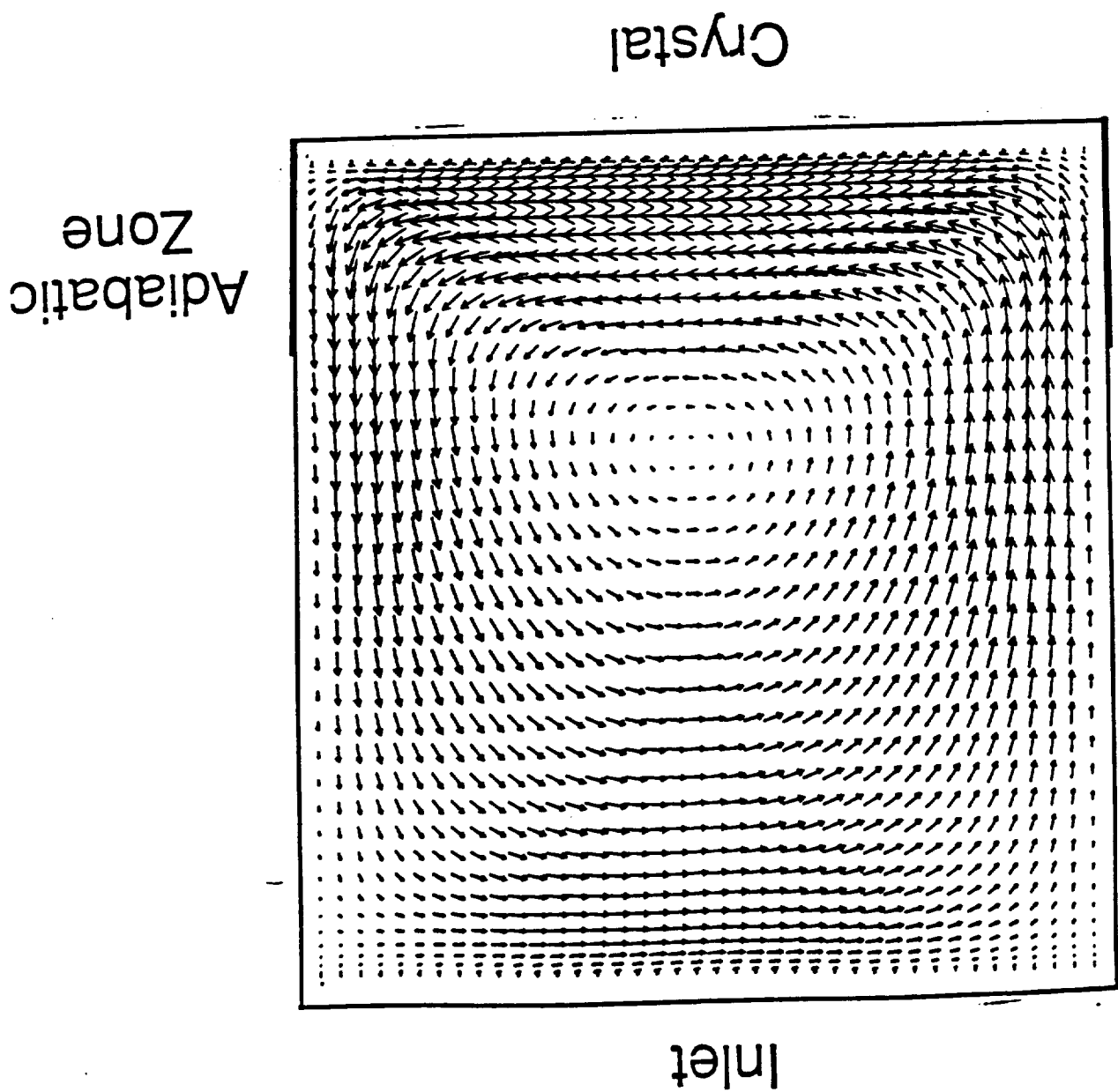
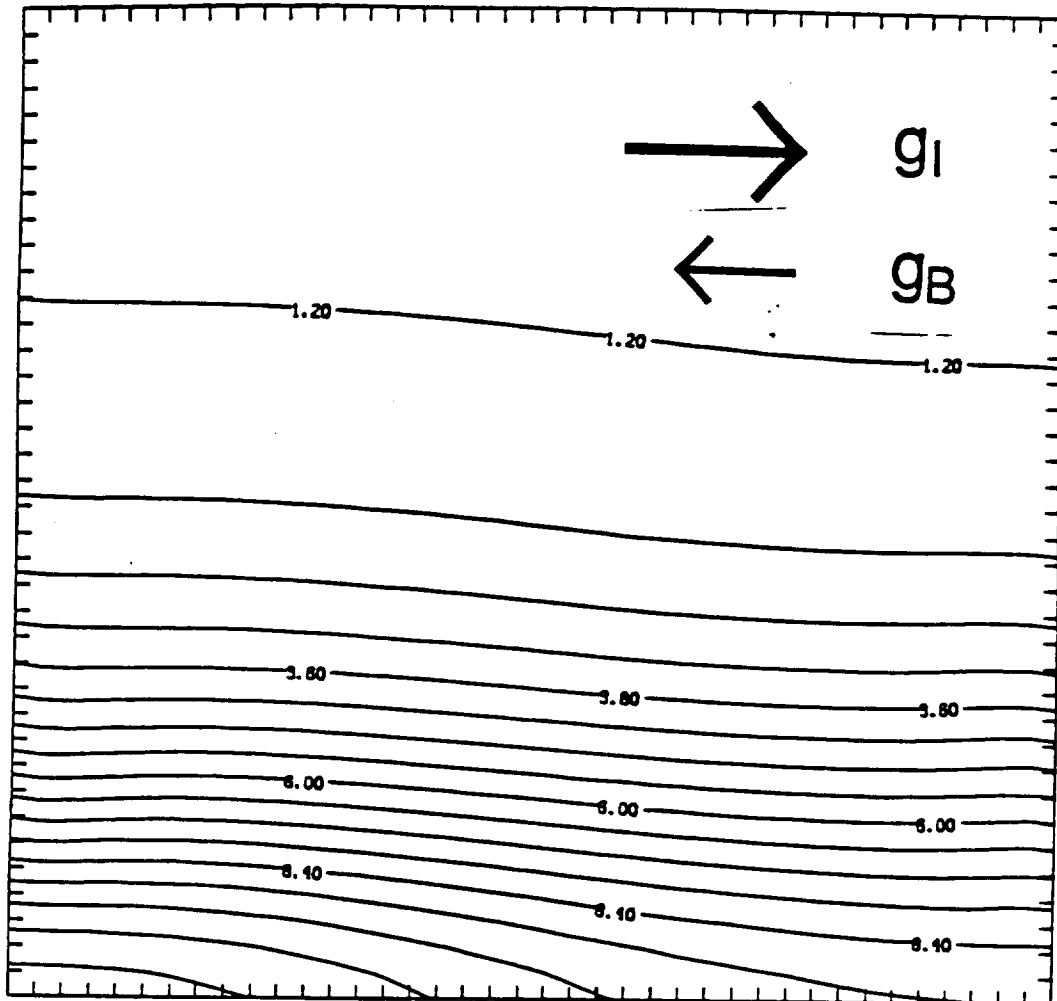


Fig. 13

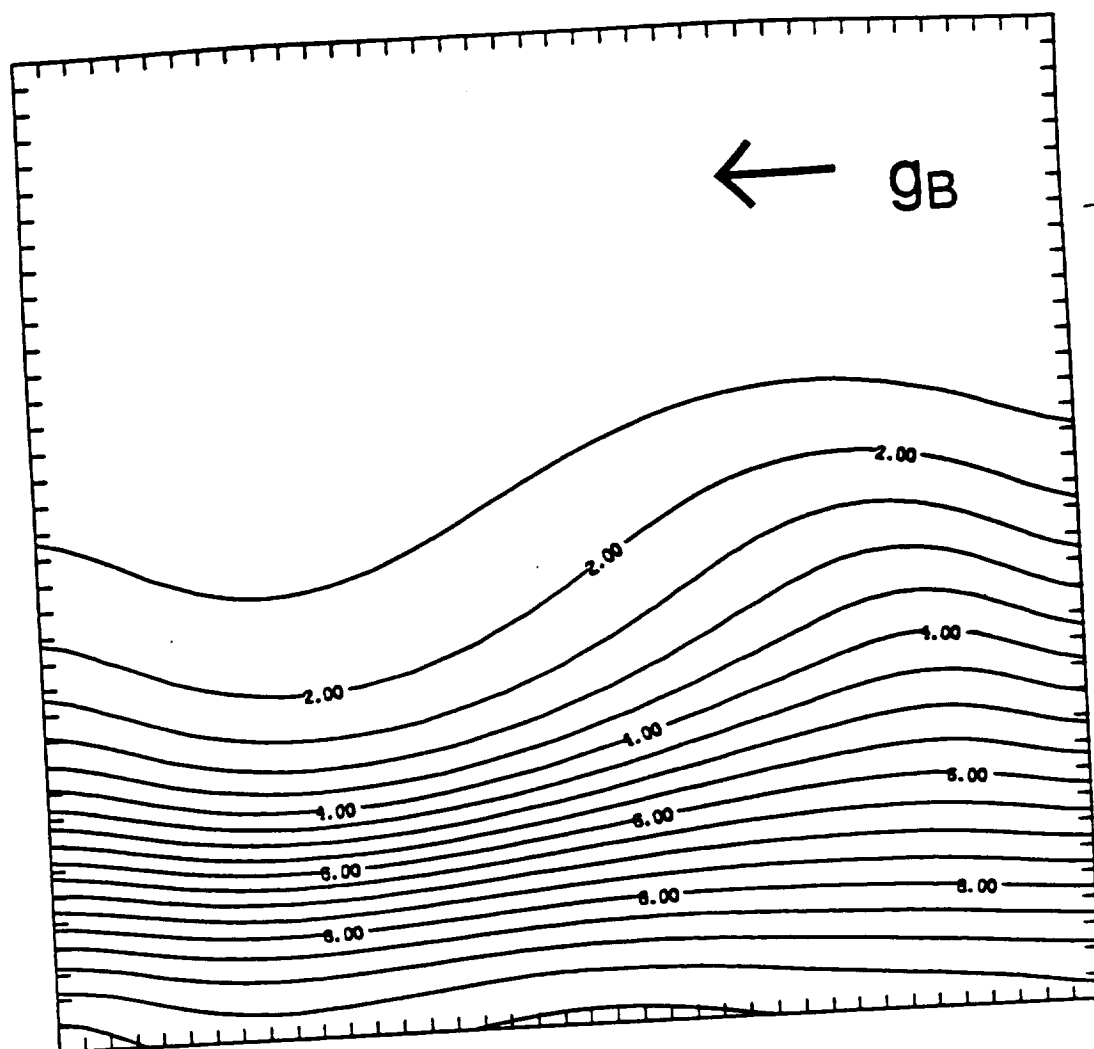


Inlet



Crystal

Inlet



Crystal

FIG. 16

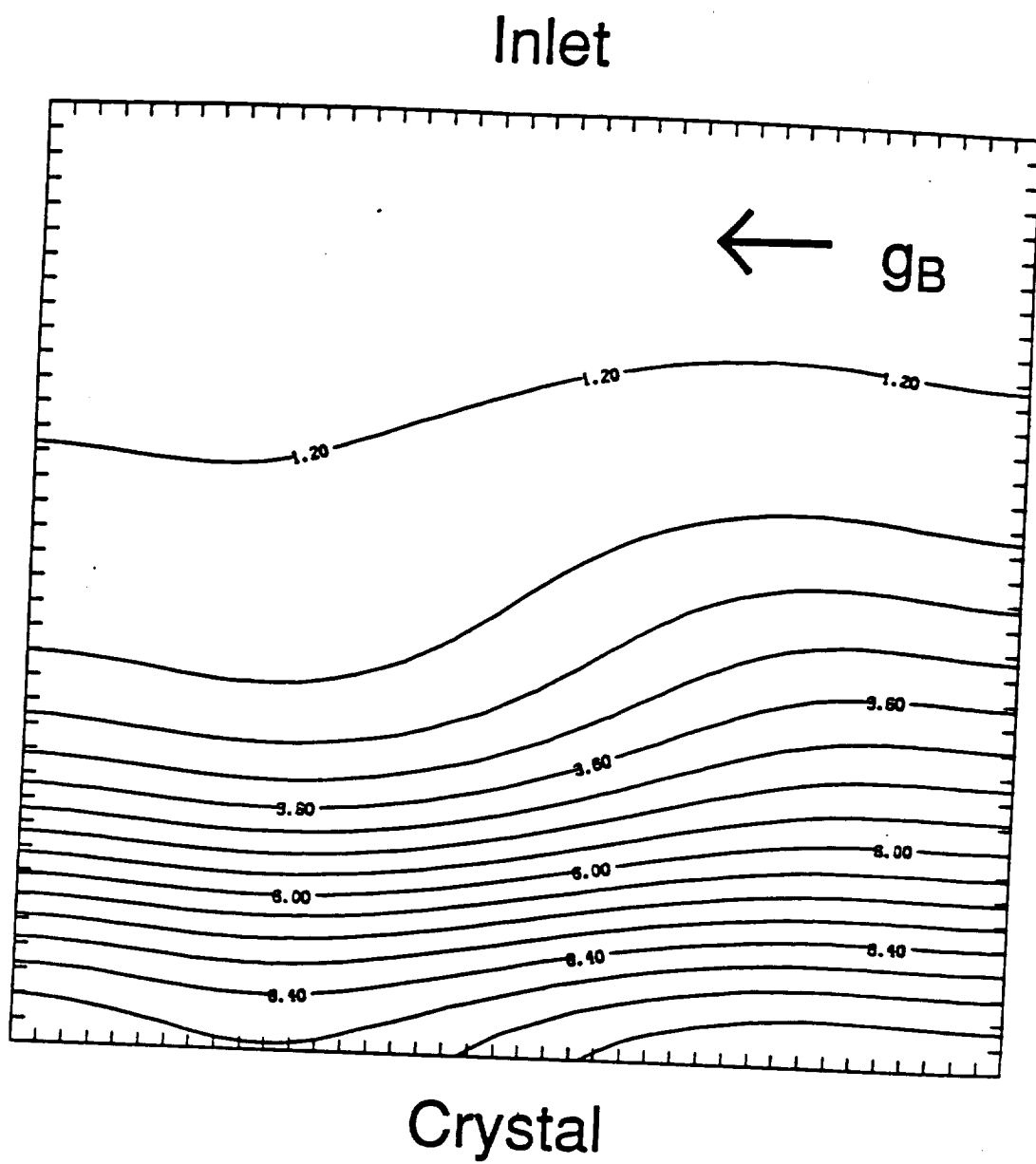
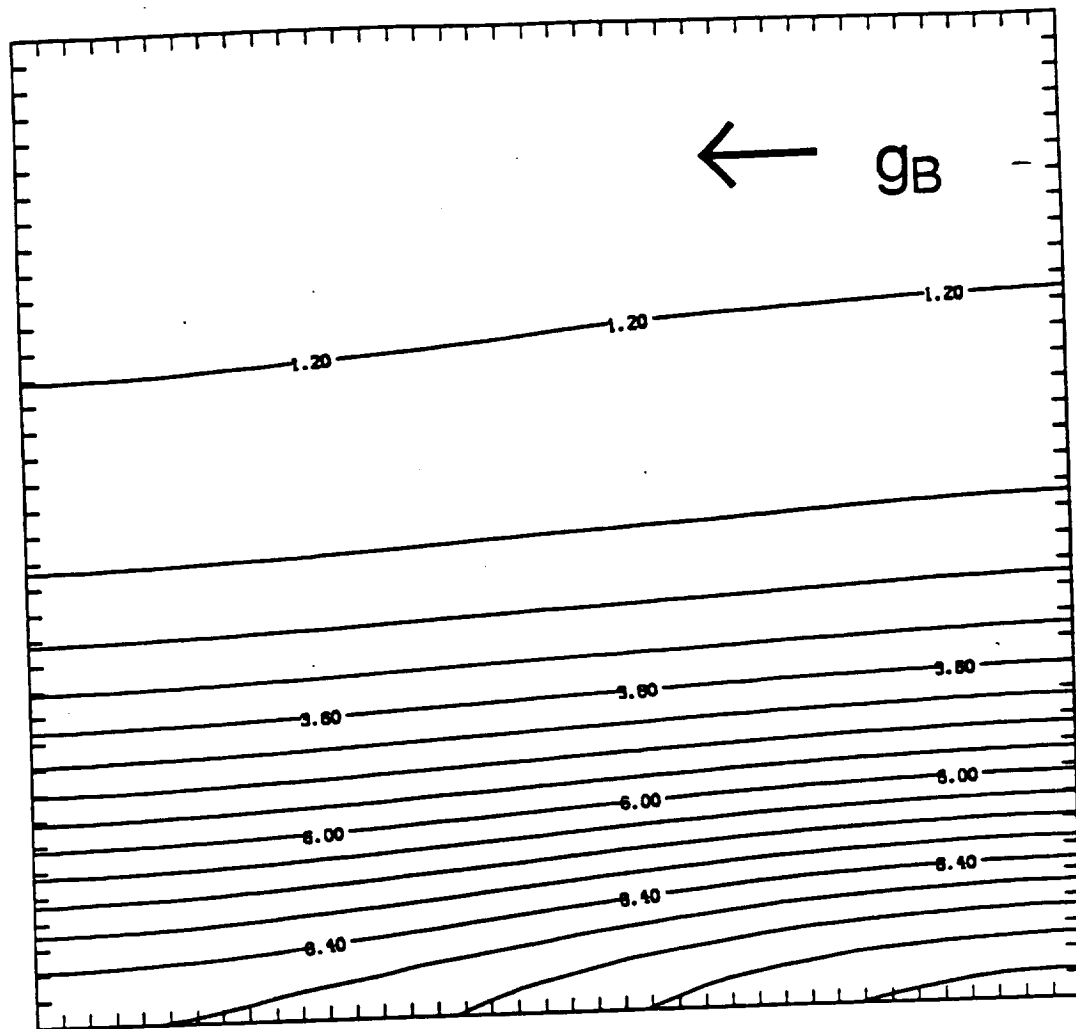


FIG. 17

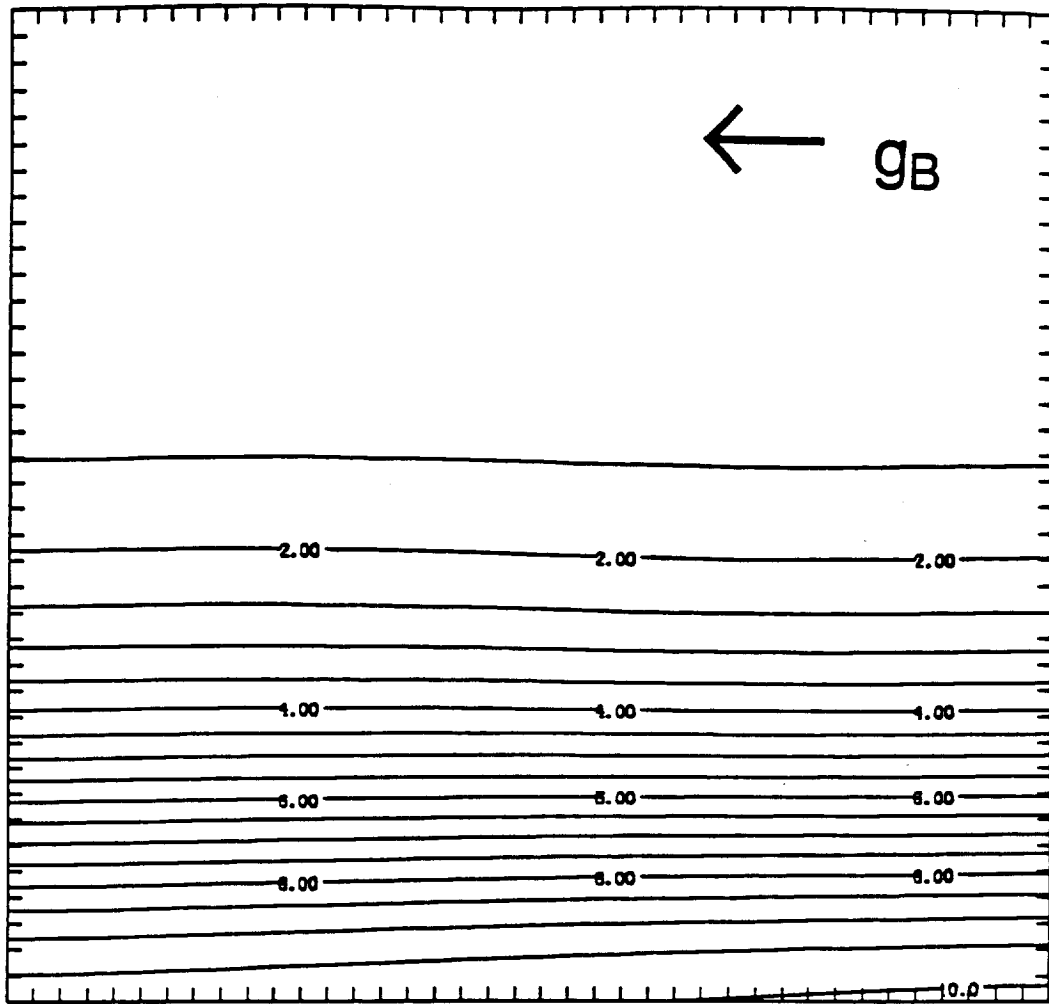
Inlet



Crystal

FIG. 18

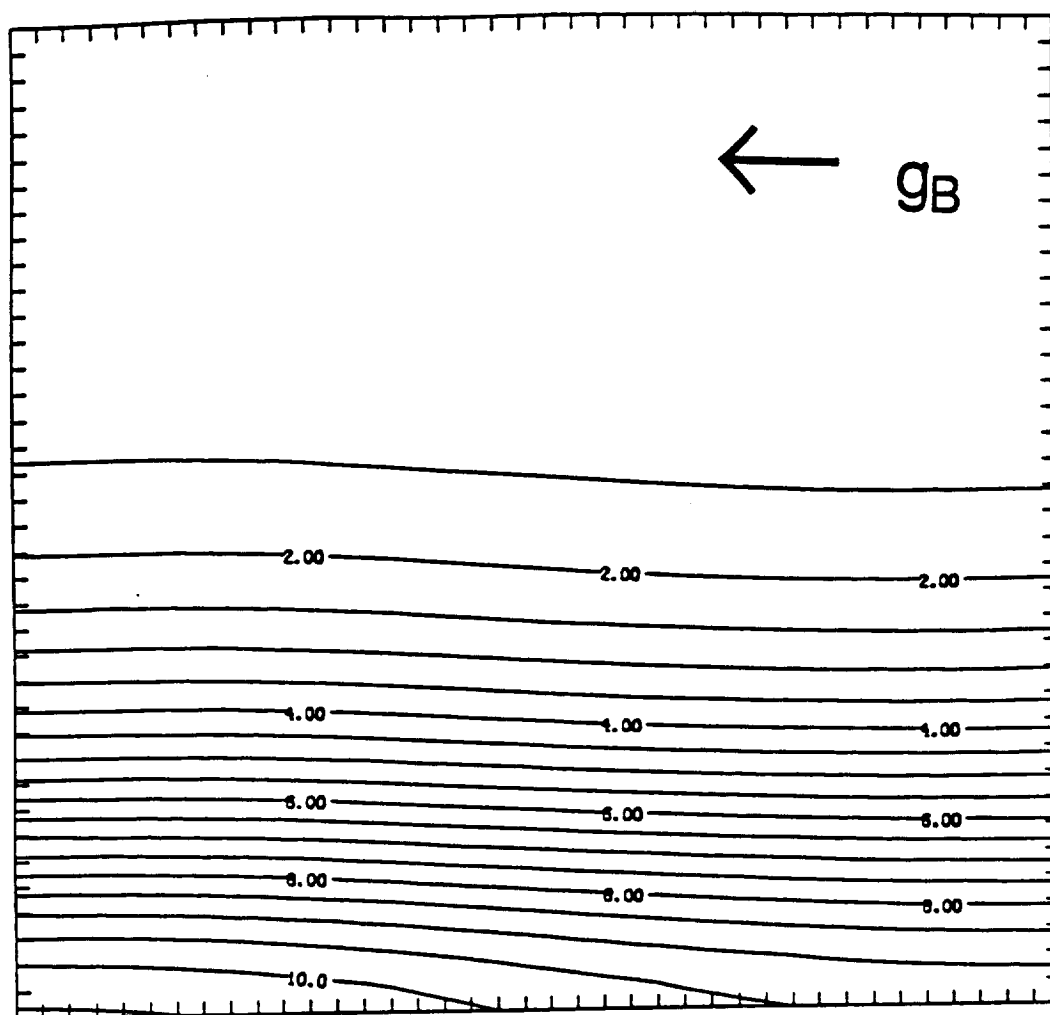
Inlet



Crystal

FIG. 19

Inlet



Crystal